1-1-1963

A 0-60 ampere current supply and the beta-gamma angular correlation of arsenic-74.

John Delbert Colclough
University of Windsor

A 0-60 AMPERE CURRENT SUPPLY AND THE β-γ ANGULAR CORRELATION OF As^{74}

BY

JOHN DELBERT COLCLOUGH

A Thesis
Submitted to the Faculty of Graduate Studies through the
Department of Physics in Partial Fulfillment
of the Requirements for the Degree of
Master of Science at
Assumption University of Windsor

Windsor, Ontario

1963

APPROVED:

E. E. Habib

F. Holuj

R. J. Thibert

ABSTRACT

A 0-60 amp. current supply is described. The ratio of the output rms. ripple current to the dc. output current is of the order of 10^{-5}%. The output current does not drift for all practical purposes and changes less than 0.01% when either the line voltage changes by 10% or thc room temperature changes by 10 C^{o}. A "fast-slow" Bell, Graham and Petch coincidence circuit is described and circuit diagrams are given for the transistorized "fast" unit. This equipment was used in conjunction with the Gerholm coincidence β-γ spectrometer to study the angular correlation between the 0.93 mev. positron group and the subsequent 600 kev. gamma ray of the decay $As^{74} \longrightarrow Ge^{74}$. The measured A_2 coefficients at energies of W = 1.8, 2.0, 2.2, 2.4 and 2.6 (relativistic units) are:

W	A	$\pm$
1.8	0.0437	0.0055
2.0	0.0045	0.00051
2.2	-0.0365	0.0072
2.4	-0.024	0.0092
2.6	-0.168	0.123

Corrections were made for scattering of the 511 kev. annihilation gammas and for the change in the 511 peak height with respect to the 600 kev. peak height when the scintillation spectrometer was rotated. The small anisotropy indicates that there is no strong K of j selection rule to reduce the contribution for matrix elements other than $\int$ Bij.

ACKNOWLEDGEMENTS

I would like to express my appreciation to Dr. E.E. Habib for his guidance and instruction throughout this work.

My thanks goes to Mr. W. Grewe for the part he played in the construction of the current supply. The assistance of Mr. R.H. Young in preparing the source and recording the data is also acknowledged. I would like to thank Miss Lee Latter for typing the manuscript. I am indebted to the National Research Council for financial support in the form of a bursary.

TABLE OF CONTENTS

LIST OF TABLES

LIST OF ILLUSTRATIONS

CHAPTER I

BETA RAY SPECTROMETERS

(i) Introduction

Magnetic beta ray spectrometers are used extensively to analyse complex nuclear spectra. They may be classified into two basic types, the flat and the helical spectrometer. In the flat type the magnetic lines of force are mainly in the direction perpendicular to the electron paths whereas in the helical instrument the lines of force are mainly in the same direction as the electron paths.

There are many problems involved with spectrometers of this type. One wishes to have a maximum luminosity (source area x transmission) while at the same time achieve a maximum energy resolution. These are, however, mutually conflicting requirements. Increasing the luminosity usually results in a decrease of the resolution and vice versa. Problems also arise regarding detector design, field shapes and power requirements.

Originally the flat spectrometers focussed electrons only in one plane while the lens spectrometers were space focussing. Today, however, nearly all flat types being used are space focussing. This is achieved by shaping the transverse field to vary as $1/\sqrt{\rho}$ where ρ is the distance to the axis of symmetry. This flat spectrometer is easy to construct and to adjust to a high resolution. The transmission can be made high ($\sim$ 0.1%) and the source and detector problems are easy to solve.

(ii) General Properties of Magnetic Spectrometers

The equation of motion of an electron moving in a plane perpendicular to a uniform magnetic field is given by:

$$B e v = \frac{m v^2}{\rho}$$

where

$$m = \frac{m_0}{\sqrt{1 - v^2/c^2}}$$

m_0 = rest mass of the electron

v = velocity of the electron

ρ = radius of electron orbit

The momentum p can be expressed, using (1), as:

$$p = mv = e.B\rho \qquad (2)$$

It is therefore convenient in experimental work to express the momentum in terms of its $B\rho$ (gauss-cm.) value. The corresponding energies can be calculated directly or obtained from tables. The relation (2) indicates that in the flat spectrometer, where ρ is constant for all energies and the field uniform, there is a linear relationship between the momentum focussed and the analysing field. Although most other spectrometers do not have constant fields over the entire trajectory, they do, however, under the conditions of fixed source, detector and baffle positions, exhibit a linear relationship between the field at any one point and the

momentum of the electrons focussed. This is also conditional upon the shape of the field remaining the same as the field B varies.

The transmission ω of a spectrometer is defined as the fraction of the electrons of momentum p emitted from the source which arrive at the detector when the instrument is focussed on p. The resolution of a spectrometer is defined with respect to its response to a source of monoergic electrons. Response curves of Figure 1.1 are obtained.

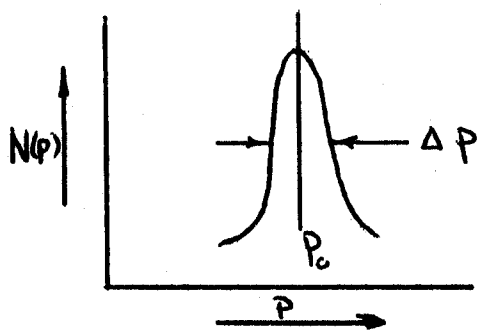

Figure 1.1

The resolution R is defined as $\frac{\Delta p}{p_0}$ where Δp is the momentum spread at half maximum and p_0 is the momentum at the peak counting rate. Since $\Delta p = K p_0$ where K is a constant, R is independent of P_0 the ratio R/ω is called the figure of merit and varies from 20 in the older instruments to 0.1 for many of the best modern ones.

(iii) Ring Focus and Baffles

In a helical (lens) type spectrometer the electron image of the source at the detector has usually a large spherical aberration. A position of minimum spherical aberration generally occurs before the electrons cross the symmetry axis. This is called the ring focus and a great improvement in performance is obtained by placing defining baffles at this point rather than at the detector. Hubert(1952) has

shown the combination of baffles, as shown by the solid lines of Figure 1.2, leads to an improvement in resolution while retaining the same transmission as other baffle systems represented by the dotted lines in Figure 1.2. The combination of diaphrams D_1, D_2, D_3 define both the solid angle and the momentum band. The diaphrams D_1 & D_3 can be replaced by a single conical baffle and D_2 by a moveable baffle. The

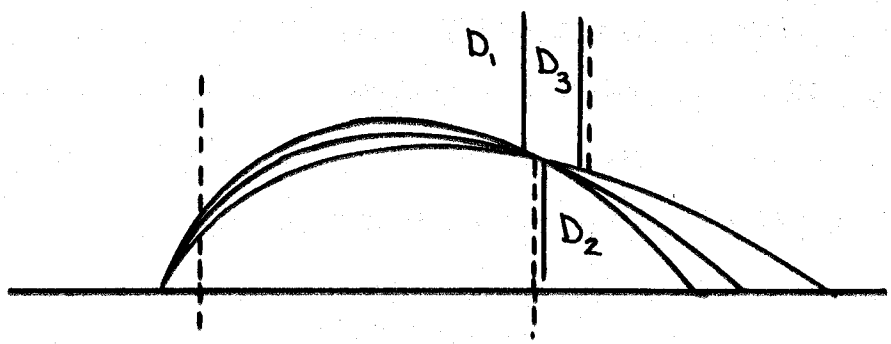

Figure 1.2 Lens Spectrometer Baffles

gap between the moveable baffle and the conical baffle defines both the transmission and resolution of the instrument. This leads to a simplified adjustment over other systems and is the type used in the first Gerholm instruments.

(iv) Response of a Spectrometer to a Monoergic Beam

The resolution R is not as convenient for making qualitative deductions as the quantity η to be defined in this section. We start with a monoergic electron beam of finite angular width emerging from a finite source. We wish to describe the response of a spectrometer to this beam. According to Gerholm (1956) the function $g(\xi, p)$ is the probability of recording an electron of momentum ξ when the instrument is set to focus electrons of momentum p. If $\xi = p$ then $g(\xi, \xi) = 1$. It can be shown that $g(\xi, p)$ is independent of p and

depends on $\frac{(\xi - p)}{p}$.

Writing $\frac{\xi - p}{p} = u$ we have:

$$\int_0^\infty q(\xi, p)\, d\xi = p \int_{-1}^{\infty} g(u)\, du = p\eta$$

This defines η which is constant for a given spectrometer depending only on the source, detector and baffle geometry.

If $N(\xi_0)$ is the intensity of the monoergic source of mean momentum ξ_0 then the counting rate $N(p)$ at a momentum setting of p will be $N(p) = \omega\, q(\xi_0, p)\, N(\xi_0)$

The peak counting rate is $\omega N(\xi_0)$. If a plot is made of $\frac{N(p)}{p}$ vs. p the area under the peak is;-

$$\int_0^\infty \frac{N(p)}{p}\, dp = \omega N(\xi_0) \int_0^\infty \frac{q(\xi_0, p)}{p}\, dp$$

Now $q(\xi, p)$ vanishes unless $p \simeq \xi_0$ and thus the effective range of integration is small. Therefore p remains roughly constant and may be moved outside the integral sign. Therefore:-

$$\text{Area under peak} = \frac{\omega N(\xi_0)}{p} \int_0^\infty q(\xi, p)\, dp$$

$$= \omega N(\xi_0)\eta$$

Thus:

$$\eta = \frac{\text{Area under peak}}{\text{Peak counting rate}}$$

In spectrometers where the peak profile is symmetric, η will be very nearly equal to the resolution R. This condition is satisfied for the Gerholm instrument using the Hubert baffle system.

(v) Response of a Spectrometer to a Continuous Distribution

For a beam of electrons of continuous distribution we introduce a shape factor $\phi(\xi)$ which is the probability per electron, that the momentum will lie in a unit interval of momentum about ξ .

With the spectrometer focussed at p the counting rate is

$$\int_0^\infty N \phi(\xi) q(\xi, p) w \, d\xi$$

Since $\phi(\xi)$ varies slowly with respect to $q(\xi, p)$ we put $\phi(\xi) = \phi(p)$ = constant over the range of integration. Then the counting rate becomes

$$N \phi(p) w \int_0^\infty q(\xi, p) \, d\xi = N \phi(p) \eta p w$$

Plotting N/p vs p the area under the curve is

$$\int \frac{N}{p} dp = \int N_0 \frac{\phi(p) \eta p w \, dp}{p} = N_0 \eta w$$

These formulas will enable us to make quantitative analysis on the observed spectra.

(vi) Lens Spectrometers

It is easily seen that an electron moving in a uniform magnetic field perpendicular to it will describe a circular orbit. If it also has a velocity component in the direction of the field, then it will describe a helical path. Such is the situation in a long lens spectrometer. The electron rotates through an angle of 360° before returning to the symmetry axis where the detector is placed. This is the simplest situation to visualize as far as lens spectrometers are concerned. The equations of motions for a homogeneous field are

according to Siegbahn (1955):

$$\ddot{r} = -\left(\frac{eB}{2m}\right)^2 r \quad ; \quad \ddot{z} = 0$$

The solution for $r(z)$ is

$$r = D \sin\alpha \sin S$$

where $$D = \frac{2mv}{eB}$$

$$S = \frac{z}{D\cos\alpha}$$

α is the angle of emission of the electron with respect to the z axis. When the paths are drawn in the rz plane it is found that the paths intersect each other rather closely within a certain region. The condition for such a ring focus is given by

$$\frac{dr}{d\alpha} = 0$$

This leads to the condition

$$\tan S / S = -(\tan\alpha)^2$$

To calculate the resolving power the width of the image at the ring focus is expressed in terms of its $B\rho$ value. The first order effect is zero we have placed the ring focus at the point where

$$dr/d\alpha = 0$$

The second order contribution is

$$\Delta r = \frac{d^2r}{d\alpha^2}\frac{(\Delta\alpha)^2}{2} + \text{other terms.}$$

$\Delta\alpha$ is half the opening angle at the source. Substituting in we get $$\Delta r = D\frac{(\Delta\alpha)^2}{2}\frac{\sin S}{\sin\alpha}\left(3 + \cos^2\alpha \cdot \tan^2 S\right)$$

The resolving power is

$$R^0 = \Delta(B\rho)/B\rho$$

Since

$$\Delta r = \frac{\partial r}{\partial D}_{(B\rho)} D \, \Delta(B\rho)$$

then

$$\Delta r = \frac{\partial r}{\partial D} D R^{\circ}$$

Substituting in we get

$$R^{\circ} = \frac{\Delta \alpha}{2} \left(3 + \cos^2 \alpha \cdot \tan^2 \delta\right)$$

The term in brackets has a broad minimum at 45°. However, due to practical considerations such as source dimensions and coil size it is found the optimum overall angle of emission is 30°. The main disadvantage with the long lens uniform field spectrometer is due to the spreading of the electron beam after passing the baffles. This requires a rather large detector thereby introducing a high background count rate. An improved design due to Siegbahn (1946) uses a fieldform which is concave upwards. Slatis and Siegbahn (1949) experimented with different field gradients and found a pronounced increase in transmission at a certain strong field gradient. In this type the electron rays cross each other at the centre and gather again at the detector. This allows a smaller counter to be used while achieving a 3 per cent transmission.

The short lens was developed before the long lens. Busch (1927) pointed out the analogy between electron optics of magnetic lenses and ordinary light optics. He calculated the focal length for short lenses as

$$\frac{1}{f} = \frac{1}{4(B\rho)^2} \int_{-\infty}^{+\infty} B_z^2 (z,0) \, dz$$

where $B_z(z,0)$ is the field component perpendicular to the lens along the axis. The field form of the short lens is drawn in Figure 1.3. Typical physical dimensions would be 15 cm long and 15 cm diameter. Resolving powers of 2.5 per cent and transmissions of 0.5% are usually obtained.

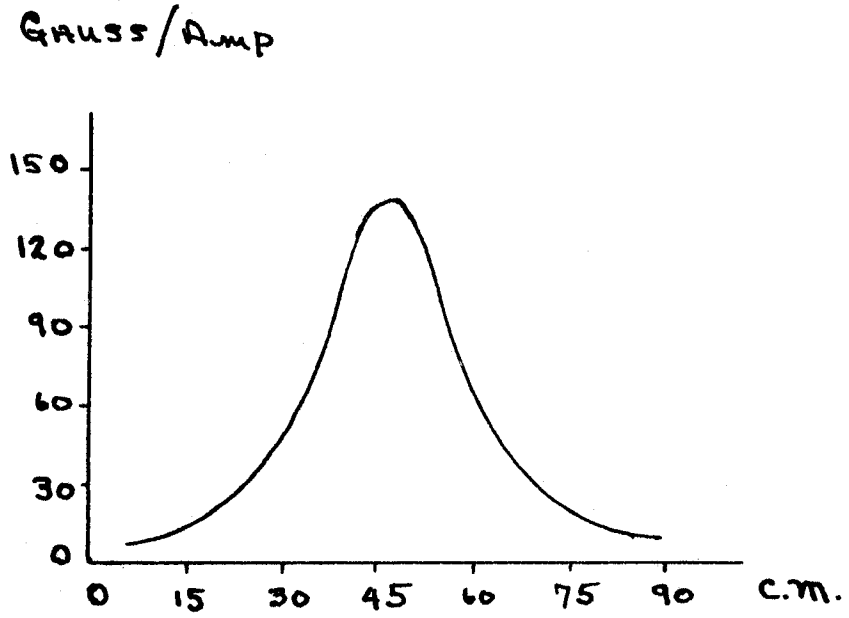

Figure 1.3 Short Lens Field Form

(vii) The Gerholm Instrument

In this instrument the two halves (see Figure 1.4b) are magnetically independent of each other. Therefore, magnetic fields of different strengths can be used in each half, thus providing the opportunity to focus simultaneously electrons of two different energies. The field form, as shown in Figure 1.5 measured along the axis increases roughly linearly with increasing distance. Theoretical (Lindgren) as well as experimental studies of the triangular field shape show that it gives a favourable high luminosity (source area x transmission) which compensates for the small geometrical dimensions of the instruments. A high transmission is very important in coincidence experiments. Sources up to 5 mm in diameter can be used without sacrifice in resolution which is 3 per cent at an effective solid angle of 3 per cent. It is also possible to convert the instrument into an electron-gamma angular correlation spectrometer. In this set (Figure 1.4a) up the average angle

of emission is reduced to reduce the correction factor for finite aperture angle. This results in a lower transmission. Typical figures for a 5 mm source are:resolution 3 per cent, transmission 1.8 per cent.

The gamma spectrometer may be rotated between the 90° and the 270° positions. Adjustments are provided so that the axis of rotation passes through the source position. The gain of the photomultiplier is affected by the external magnetic field of the beta lens. The peak position of the 511 kev. annihilation gamma decreases 2.5 channels (25 kev.) on the kicksorter when the spectrometer is rotated from the 180° to the 90° position.

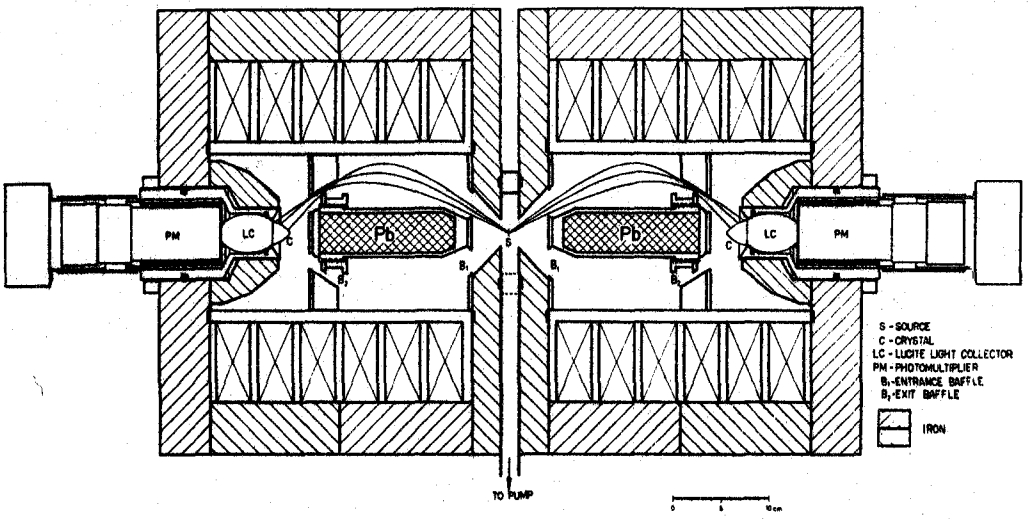

Figure 1.4b Electron - Electron Spectrometer

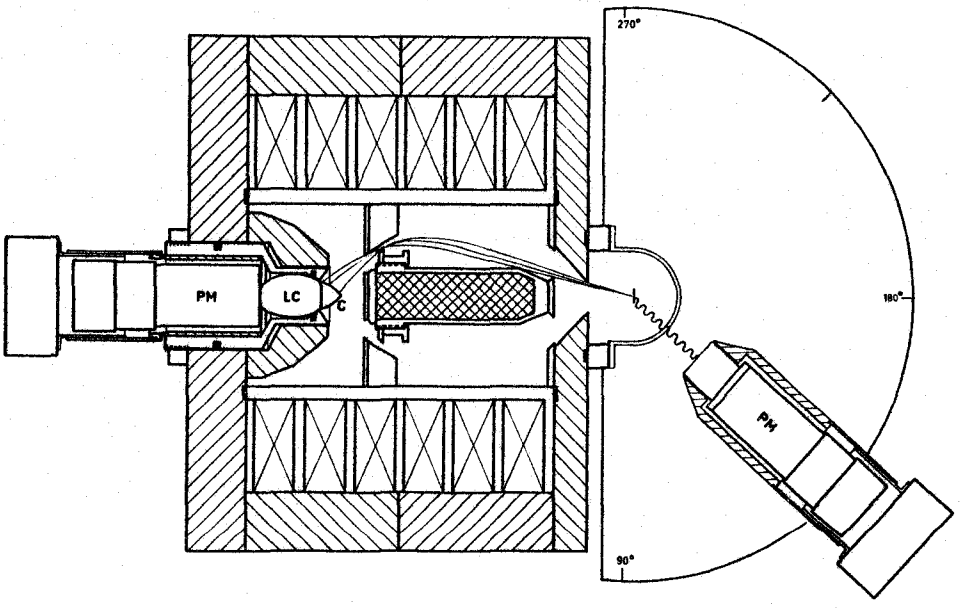

Figure 1.4a Angular Correlation Spectrometer

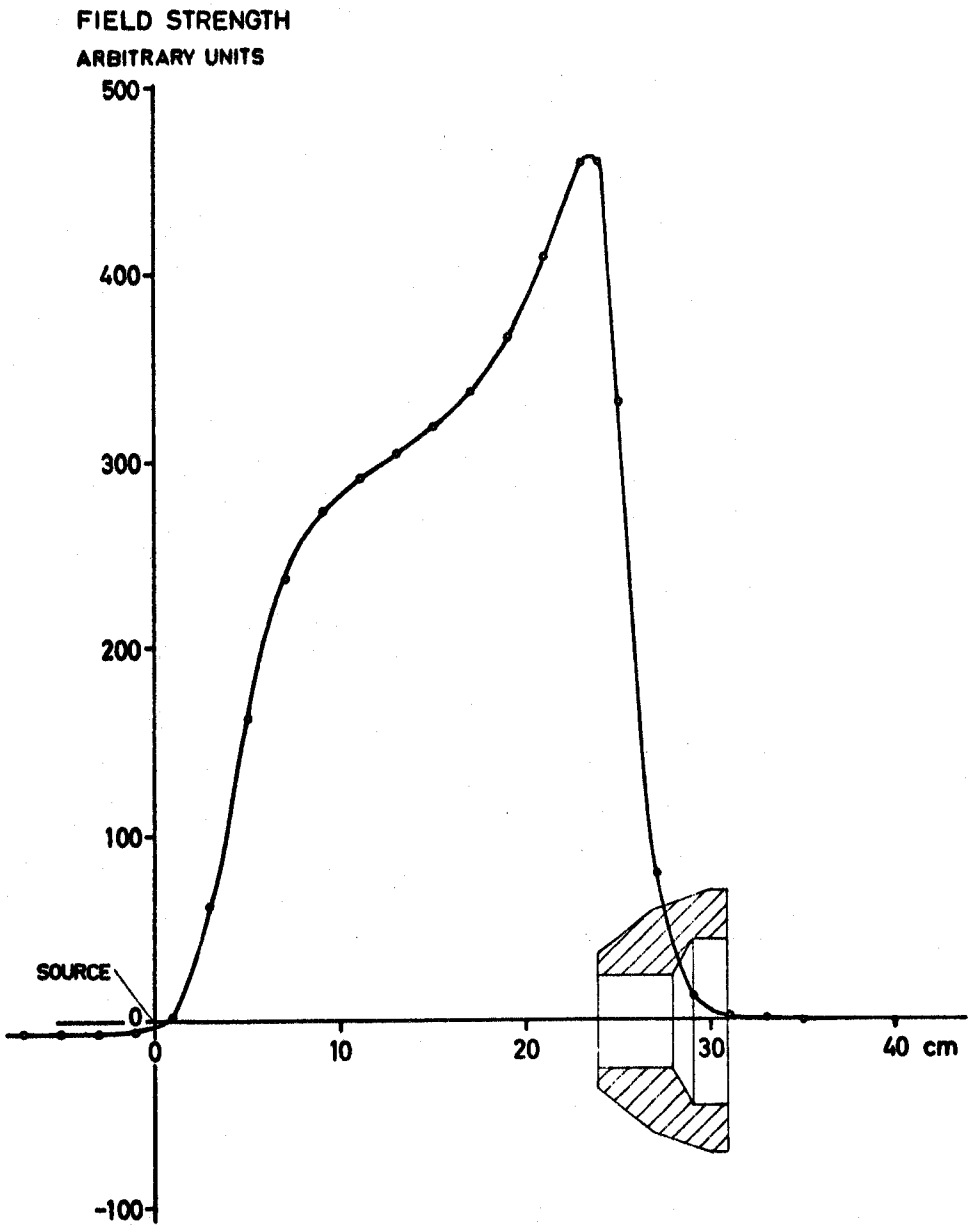

Figure 1.5 Field Form of the Gerholm Instrument

CHAPTER II

β-γ ANGULAR CORRELATIONS

(i) Introduction

β-γ angular correlations have two main areas of application. One is to test the fundamental laws of nature such as parity nonconservation and the other is to study nuclear structure. The formulas for the β-γ angular correlation are expressed in terms of certain nuclear matrix elements. We gain insight into the nuclear structure by knowing the relative magnitudes of the nuclear matrix elements responsible for the beta transition.

The first article on β-γ angular correlation theory was published by Falkoff and Uhlenbeck (1950). Since then a great many experimental and theoretical works have been performed. Notable accomplishments are the analysis of Sb^{124} (Hartwig and Schopper) and Pr^{144} (Steffen). Konopinski (1959) has written a review article on allowed transitions and Weidenmuller (1961) has published an article on first forbidden transitions. An excellent survey of the literature may be found in his paper. Kotani (1959) has also written an article on the deviations from the ξ approximation.

When two particles are emitted simultaneously from a nucleus an angular correlation between their directions of emission can in principle be obtained. The form of the correlation function $W(\Theta)$ depends only on the angular momenta of the nuclear states involved and of the outgoing particles. It is of the form $W(\Theta) = 1+A_2P_2\cos(\Theta)$

for first forbidden transitions. To determine A_2 theoretically requires more detailed information concerning the interactions describing the decay process. All allowed transitions have isotropic β-γ angular distributions and if the shape of an energy spectrum is strictly identical to that for an allowed case then the distribution will be also isotropic.

Many nonunique first forbidden transitions, $\Delta J = 0, 1$; $\Delta L = 1$; $\Delta \pi = (-)$, have allowed shape beta ray energy spectra. The ξ approximation is applicable to this case. In this approximation the coulomb energy of the electron at the nuclear radius is larger than the total energy of the electron. Mathematically we have

$$\frac{\alpha Z}{R} >> W_0$$

where

W_0 = max. β-ray energy

R = nuclear radius

α = fine structure constant

Z = no. of protons

The measurable quantities in the ξ approximation do not give us enough information to determine the nuclear matrix elements uniquely. We find, however, that valuable relations among the nuclear matrix elements may be gained by considering nonunique first forbidden transitions which show deviations from the ξ approximation. The unique first forbidden transitions, $(\Delta J = 2)$ have a unique energy spectrum. There is only one nuclear matrix element contributing to the transition i.e. the B_{ij} term. In this case both the energy and angular dependence of all measurable quantities are determined. In the nonunique transitions showing deviations from the ξ approximation there is a possibility that the contribution from matrix elements other than the B_{ij} term is

small. In this case we expect the nonunique transitions to behave similarly to the unique transitions. To explain this situation a selection rule is introduced which inhibits contributions from matrix elements other than $\int \beta_{ij}$.

(ii) Selection Rule Effect

The Hamiltonian describing the weak interaction in β decay is of the form

$$H_\beta = \left(O O_L \tau_+ \tau_+^L + O^\dagger O_L^\dagger \tau_- \tau_-^L \right) \delta(\bar{r} - \bar{r}_L)$$

where $\bar{r}$ and $\bar{r}_L$ are the nucleon and lepton position vectors. τ_+ is the operator in i spin space which transforms a neutron to a proton and τ_+^L is the operator, in i spin space for leptons, which transforms a neutrino into a negatron. The Hermitian conjugates τ_- and τ_-^L make the reverse transformations. O and O_L are operators which act on the nucleon and lepton wave functions respectively. We would like to know the form of O and O_L.

The Hamiltonian, H_β , must be invariant under Lorentz transformations, including rotations and translations of the axes. Conservation of angular momentum is also required. These restrictions indicate that the Hamiltonian must be a linear combination of scalars and pseudoscalars. The scalars and pseudoscalars can be constructed from the lepton and nucleon wave functions in five different ways. The wave functions are multiplied by 4 $\times$ 4 matricies which are constructed from five independent matricies. There are two sets in common use. One set is $\alpha \ (= \alpha_1, \alpha_2, \alpha_3)$, β, 1 and the other corresponding set is $\gamma_1, \gamma_2, \gamma_3, \gamma_4, 1$. An important product matrix is $\gamma_5 = \gamma_1 \gamma_2 \gamma_3 \gamma_4 = -i \alpha_1 \alpha_2 \alpha_3$. There are also three products $\sigma = \alpha \gamma_5$. As an example consider

the vector interaction. The four quantities $(\phi \gamma_4 \gamma_\mu \psi)_{\mu = 1,2,3,4}$ form a four-vector. The scalar product of two such vectors is invariant and hence a possible combination of O's and O_i's leads to

$$\sum_\mu (\bar{\Psi}_f \gamma_4 \gamma_\mu \Psi_i)(\psi_f \gamma_4 \gamma_\mu \psi_i)$$

which is a scalar matrix element. $\bar{\Psi}_f$ and $\bar{\Psi}_i$ denote the final and initial nucleon wave functions respectively while ψ_i and ψ_f denote the initial and final lepton wave functions respectively. A pseudoscalar is the "scalar" product of a vector and a pseudovector. A suitable pseudovector is $(\phi \gamma_4 \gamma_\mu \gamma_5 \psi)_{\mu = 1,2,3,4}$. Hence a possible interaction matrix is

$$\sum_\mu (\bar{\Psi}_f | \gamma_4 \gamma_\mu | \Psi_i)(\psi_f \gamma_4 | c \gamma_\mu + c' \gamma_\mu \gamma_5 | \psi_i)$$

This is called the vector interaction. The pseudovector interaction is given by

$$\sum_\mu (\bar{\Psi}_f | \gamma_4 \gamma_\mu \gamma_5 | \Psi_i)(\psi_f \gamma_4 | c \gamma_\mu \gamma_5 + c' \gamma_\mu | \psi_i)$$

The c and c' are coupling constants.

The five possible forms of interactions are known as the scalar, the pseudoscalar, the vector, the axial-vector, and the tensor interaction. It has been established (Weidenmuller) that the vector and axial-vector interactions are responsible for the beta decay.

Following Weidenmuller (1961) the Hamiltonian for the V-A (vector -- axial-vector) interaction is

$$H_\beta = \sum_i \sum_\mu \int \left[\bar{\Psi}_f \gamma_4^{(i)} \gamma_5^{(i)} (C_V - C_A \gamma_5) \tau_i \Psi_i\right] \times \left[\psi_f \gamma_4 \gamma_\mu (1 + \gamma_5) \psi_i\right] d\tau + \text{Herm. conj.}$$

The various forbidden matrix elements are found by expanding the second square bracket and taking into account nuclear matrix elements of the order v/c.

For the vector interaction the first square bracket gives rise to matrix elements $\int 1$ and $\int \alpha$. Here α is of the order of v/c and has the selection rule $\Delta J = 0, \pm 1$ ($0 \not\to 0$), $\Delta \pi = -1$, which is forbidden while $\int 1$ is an allowed matrix element. In the expansion of the second bracket we keep terms of the order $g\bar{r}$ and $k\bar{r}$ where g and k are the neutrino and electron momentum respectively. Thus, the matrix element $\int 1$ becomes $\int \bar{r}$ which obeys the selection rule for first forbidden decay. Corresponding terms of order $\bar{r}$ in the matrix element $\int \alpha$ would lead to second forbidden matrix elements. Thus, the two forbidden matrix elements originating from the vector interaction are $\int \alpha$ and $\int \bar{r}$.

The axial vector interaction consists of two parts, $\int \sigma$ and $\int \gamma_5$. The σ is an allowed matrix element. Keeping terms of the order $g\bar{r}$ and $k\bar{r}$ in the second bracket leads to three first forbidden matrix elements from the $\int \sigma$ matrix.

These are:

$$\int \sigma \cdot \bar{r} \quad ; \quad \int [\sigma \times \bar{r}]$$

and

$$\int B_{ij} = \int \left[\sigma_i x_j + x_i \sigma_j - \tfrac{2}{3} \delta_{ij} (\sigma \cdot \bar{r}) \right]$$

$\int \gamma_5$ is already first forbidden being of order v/c. Thus, the axial vector interaction gives rise to four first forbidden matrix elements. The six first forbidden matrix elements, with their selection rules and common notations, are given in Table 1.

The rank λ of the nuclear matrices appearing in

TABLE 1

First Forbidden Matrix Elements

Symbol	Matrix Element	ΔJ	$\Delta\pi$
ηw	$C_A \int \bar{\sigma}\cdot\bar{r}$	0	-1
$\eta \xi' v$	$C_A \int i\gamma_5$		
ηx	$-C_V \int \bar{r}$	$0, \pm 1$ no $(0 \to 0)$	-1
$\eta \xi' y$	$-C_V \int i\alpha$		
ηu	$C_A \int i\bar{\sigma}\times\bar{r}$		
ηz	$C_A \int B_{ij}$	$0, \pm 1, \pm 2$ no $(0 \to 0)$ no $(1 \to 0)$ no $(0 \to 1)$	-1

where

$$|\eta|^2 = \left| C_A \int B_{ij} \right|^2$$

each β decay has to satisfy

$$|J_0 - J_1| \leq \lambda \leq J_0 + J_1 \qquad -(2)$$

where J_0 and J_1 stands for the initial and final nuclear spin in β decay. It is convenient to introduce two parameters X_1 and Y_1. These are defined as follows:

$$X_1 = \xi' v + \xi w \qquad \text{for } \lambda = 0$$

$$Y_1 = \xi' y - \xi(u+x) \qquad \text{for } \lambda = 1$$

These replace the relativistic nuclear matrix elements v and y.

ie. $v \longrightarrow X_1$

$y \longrightarrow Y_1$

In the ξ approximation the following relation is satisifed:

$$|X_1| \sim |Y_1| (\sim \xi) >> |w| \sim |u| \sim |x| \sim |z|.$$

Under the selection rule effect we ask that the parameter z become of the same order as, or larger than, X_1 and Y_1. This may be understood in two possible ways depending on which nuclear model is applicable. One is known as the "K selection rule" while the other is the "j selection rule."

The K forbiddenness was introduced by Alaga, Alder, Bohr and Mottelson (1955). K is the component of the nuclear total angular momentum J on the nuclear axis of symmetry. The rank λ must satisfy relation (2) above as well as (3) below

$$|K_0 - K_1| \quad \Delta K \leq \lambda \leq K_0 + K_1$$

for a transition

$$(K_0, J_0, \pi_0) \longrightarrow (K_1, J_1, \pi_1)$$

The regions of application which have been established for this model are $150 < A < 190$ and $A > 225$.

The j selection rule is due to the configuration character of the Mayer-Jensen shell model. Here j is the total angular momentum of a nucleon in a shell. For j forbiddenness one considers nuclei in the region $50 \leq Z$; $N \leq 82$. In the Mayer-Jensen model nucleons outside the closed shell $Z = N > 50$ belong to the $h_{11/2}$, $g_{7/2}$, $d_{5/2}$, $d_{3/2}$ and s states. Among these only the $h_{11/2}$ state has odd parity. Since the first forbidden transitions change parity the number of nucleons which occupy the h state has to be changed by one unit during the decay. Therefore, we must have a $\Delta j \geq 2$ and the available nuclear matrix element with $\lambda = 2$ makes the major contribution. Thus, in j forbiddenness we have the relations

$$|Z| > |X|, |U| \text{ and } |W|.$$

j forbiddenness cannot be applied where N and Z belong to different major shells.

Matumoto, Morita and Yamada (1955;1958) have suggested examining the case where $Z \neq 0$, $X \neq 0$, $Y \neq 0$, but $X = U = W = 0$. This is called the modified B_{ij} approximation.

(iii) Relations Between X and Y under the Modified B_{ij} Approximation

We will in this section consider results only for a decay scheme of the type shown in Figure 2.1.

In the modified B_{ij} approximation we need only two parameters. They are as follows:

$$X = \frac{\left[\pm \frac{\alpha Z}{2R} \, i \int \bar{G} \cdot \bar{r} - \int \gamma_5 \right]}{i \left(\int B_{ij} \right)_2}$$

and

$$Y = \frac{\left[\pm \frac{\alpha Z}{2R} \, C_A \int \bar{G} \times \bar{r} + \left(\frac{\alpha Z}{2R} \right) i \, C_V \int \bar{r} \mp C_V \int \bar{\alpha} \right]}{i \, C_A \left(\int B_{ij} \right)}$$

X and Y are similar to X_1 and Y_1 defined previously and are the relative magnitude of the contributions from matrices of rank zero and one with respect to $\int B_{ij}$. In the decay scheme of Figure 2.1

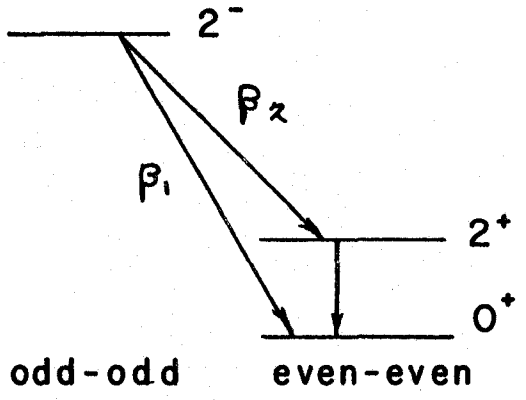

Figure 2.1 $2^-(\beta)2^+(\gamma)0^+$ Decay Scheme

the beta-gamma directional correlation is given as in equation (1) with an isotropy (Matumoto et al. 1963).

$$A_2 = \frac{p^2\left[-\frac{1}{2}\left(\frac{3}{7}\right)^{1/2}X + \frac{3}{4}\left(\frac{1}{14}\right)^{1/2}Y - \frac{3}{224}W\right]}{W\left[X^2+Y^2+\frac{1}{2}\left(\frac{1}{21}\right)^{1/2}\left(\frac{p^2}{W}\right)X - \frac{1}{4}\left(\frac{1}{14}\right)^{1/2}\left(\frac{p^2}{W}\right)Y + \left(\frac{1}{12}\right)q^2 + \left(\frac{59}{672}\right)p^2\right]}$$

If we measure A_2 at a certain energy and insert this in the above equation we will obtain a relation between X and Y which is a circle in the X-Y plane. It is

$$(X - X_0)^2 + (Y - Y_0)^2 = R^2$$

where

$$X_0 = \frac{-\left(\frac{1}{4}\right)\left(\frac{1}{21}\right)^{1/2}\frac{p^2}{W}\left[3 + A_2(W)\right]}{A_2(W)}$$

$$Y_0 = -\left(\frac{1}{2}\right)\left(\frac{1}{21}\right)^{1/2}X_0$$

$$R^2 = X_0^2 + Y_0^2 + \left(\frac{W}{8}\right)\left(\frac{3}{7}\right)^{1/2}X_0 - \left(\frac{1}{12}\right)\left(q^2+p^2\right)$$

We would like to obtain values for X and Y. In principle we could obtain X and Y experimentally from two different experiments and compare the results with theoretical calculations. The latter calculations do, however, require more precise knowledge of the nuclear radial wave function than we have available. Instead we can get a second relation between X and Y which is dependent on the branching ratio (which can be determined experimentally) and the ratio

$$\left(\sum B_{ij}\right)_1 \Big/ \left(\sum B_{ij}\right)_2$$

This ratio is dependent on the nuclear model assumed. The second relation is again a circle in the X-Y plane and is given by

$$X^2 + Y^2 = R'^2$$

where

$$R'^2 = \frac{f_{c_2}}{f_2}\left[\frac{a_2 f_{c_1}}{5 a_1 f_{c_2}}\left|\frac{(\sum B_{ij})_1}{(\sum B_{ij})_2}\right|^2 - 1\right]$$

a_1 and a_2 are the branching ratios for the β_1 and β_2 transitions while f_2, f_{c_1}, and f_{c_2} are the integrated Fermi functions for β_2 decay and the corrected integrated fermi functions for β_1 and β_2 decay respectively. These are given by Matumoto et al. (1963). If X and Y have solutions, i.e. if the two circles cross each other, then the assumed nuclear model is realized. In this way, we can test each nuclear model to find the configuration of the 2^+ states.

(iv) Calculation of $(\sum B_{ij})_1 / (\sum B_{ij})_2 = M$

For rotational excitation of the collective model (K selection rule) the ratio is:-

$$M = \left(\frac{7}{2}\right)^{1/2}$$

This is constant for all nuclei having decay schemes of Figure 2.5

For the j-j coupling shell model (j selection rule) the calculation of M is more difficult. Results are given by Matumoto et al. (1963).

They are as follows:

(i) for protons excited:

$$M = (-1)^{j_p - j_n}\frac{\left[\pi(2j_p - 1)/10(2j_p + 1)(2j_p + 1 - \pi)\right]^{1/2}}{\left[W(22 j_p j_p, 2 j_n)\right]}$$

(ii) for neutrons excited:

$$M = (-)^{1+j_p-j_n} \frac{\left[(2j_n-1)(2j_n+1-r)/10r(2j_n+1)\right]^{1/2}}{\left[W(22j_n j_n, 2j_p)\right]}$$

CHAPTER III

THE CURRENT SUPPLIES

(i) Introduction

Two solid state 0-60 amp. current supplies have been built in this laboratory to provide current for the Gerholm coincidence spectrometer. The ratio of the rms. ripple current on the output to the dc. output current is of the order of $10^{\cdot 5}$%. The output current does not drift for all practical purposes and changes less than 0.01% when either the line voltage changes by 10% or the room temperature changes by 10 C^{o}

The block diagram of the supply is shown in Figure 3.1. There are two feedback systems, -the fast feedback system, which controls the current, and the servo system which controls the variacs so that there is always 3 volts across the 2N278 series regulating power transistors. Three phase 117 volt 60 cycle power is fed to three ganged General Radio Variacs. The output from the variacs goes to a three phase full wave rectifier. The rectifier output is filtered by a 10,000 uf. capacitor. Current passes from the positive to negative terminals of the filter through a series connected resistor chain consisting of the spectrometer coils, the 0.15 ohm standard resistor, and the 10 2N278 power transistors. Overload protection for the 10 parallel connected 2N278's is provided by an 8 volt zener diode connected as shown in Figure 3.3.

(ii) The Reference Supplies

The 9.3 volt output from the reference supplies changes less than 0.01% when the input rms. voltage is changed from either 117 to 128

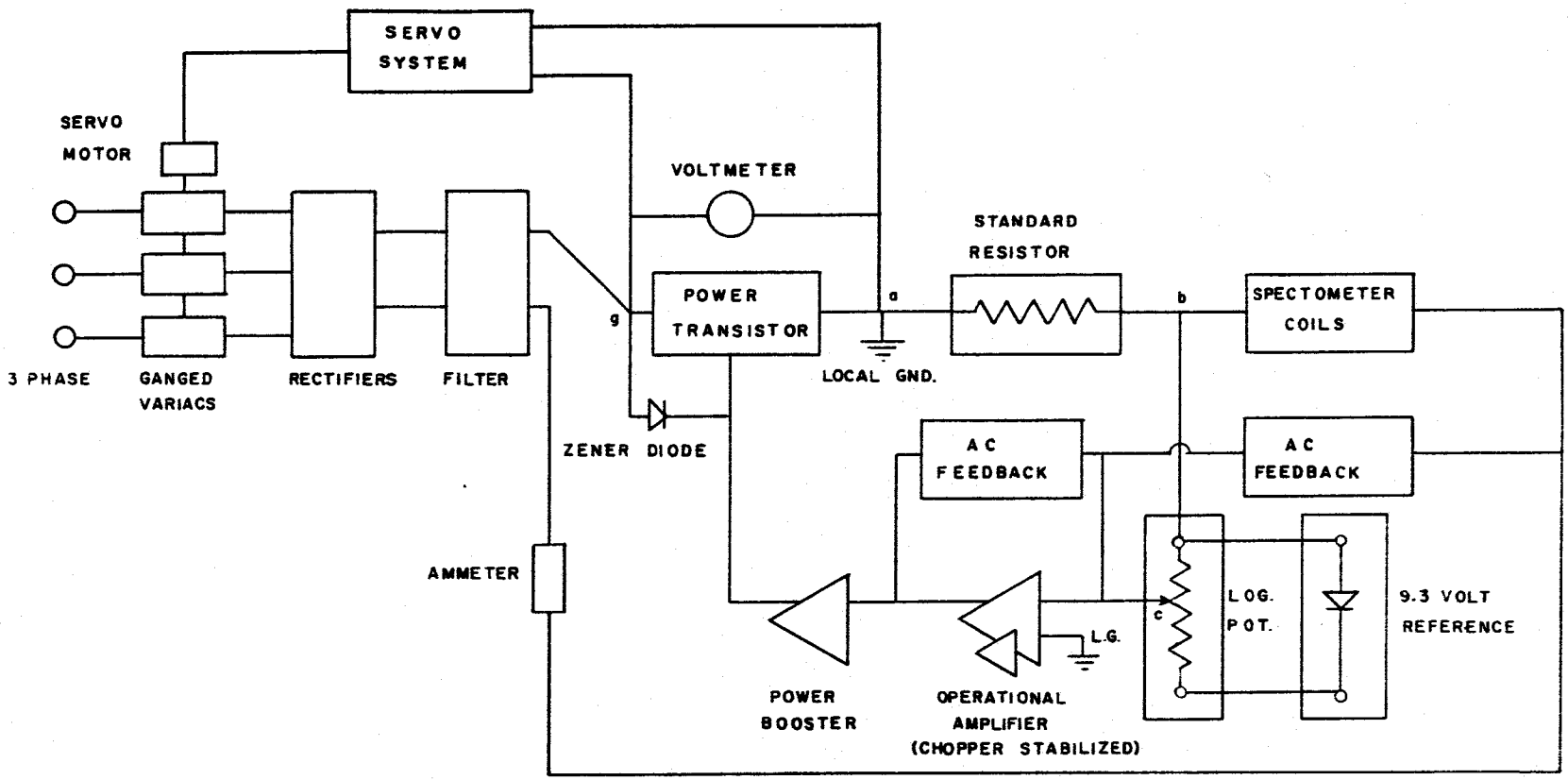

FIGURE 3-1 BLOCK DIAGRAM CURRENT SUPPLY

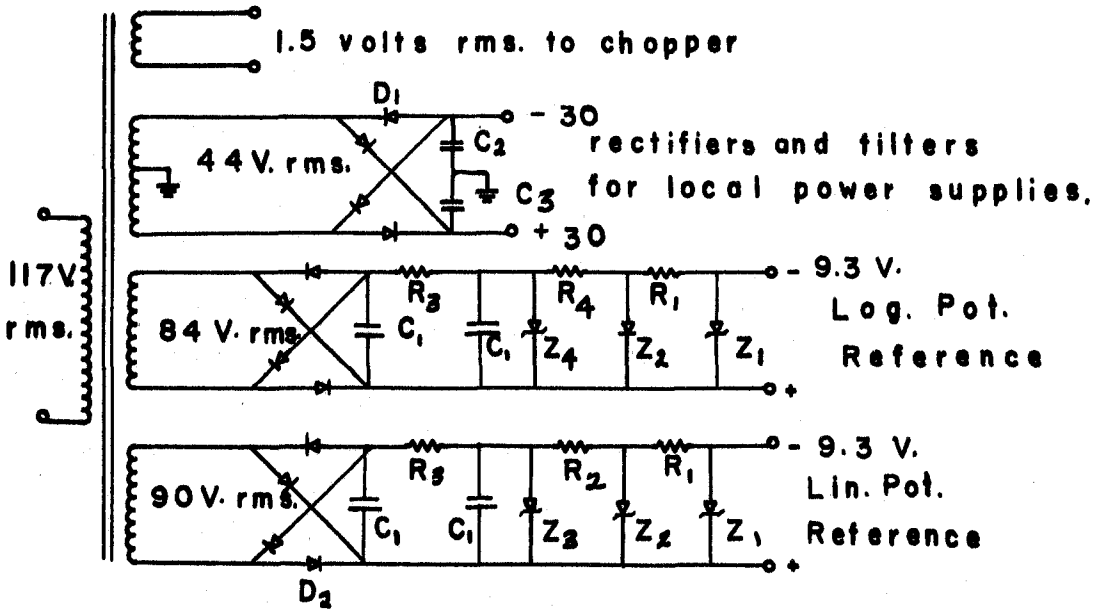

C_1 = 100 uf., 150 VDC.

C_2 = 3000 uf., 50 VDC.

C_3 = 1500 uf., 50 VDC.

D_1 = 10J2 Diode

D_2 = F2 Diode

Z_1 = IN2623 9·3V temp. compensated zener diode.

Z_2 = 2×IN2621 = 18V " " " "

Z_4 = IN2836 82 V, 50 WATT zener diode.

Z_3 = IN2833B 62V, " " " "

R_1 = 900 ohms, R_2 = 2·2 K, R_3 = 680 ohms, R_4 = 3·3 K

REFERENCE SUPPLIES

FIGURE 3·2

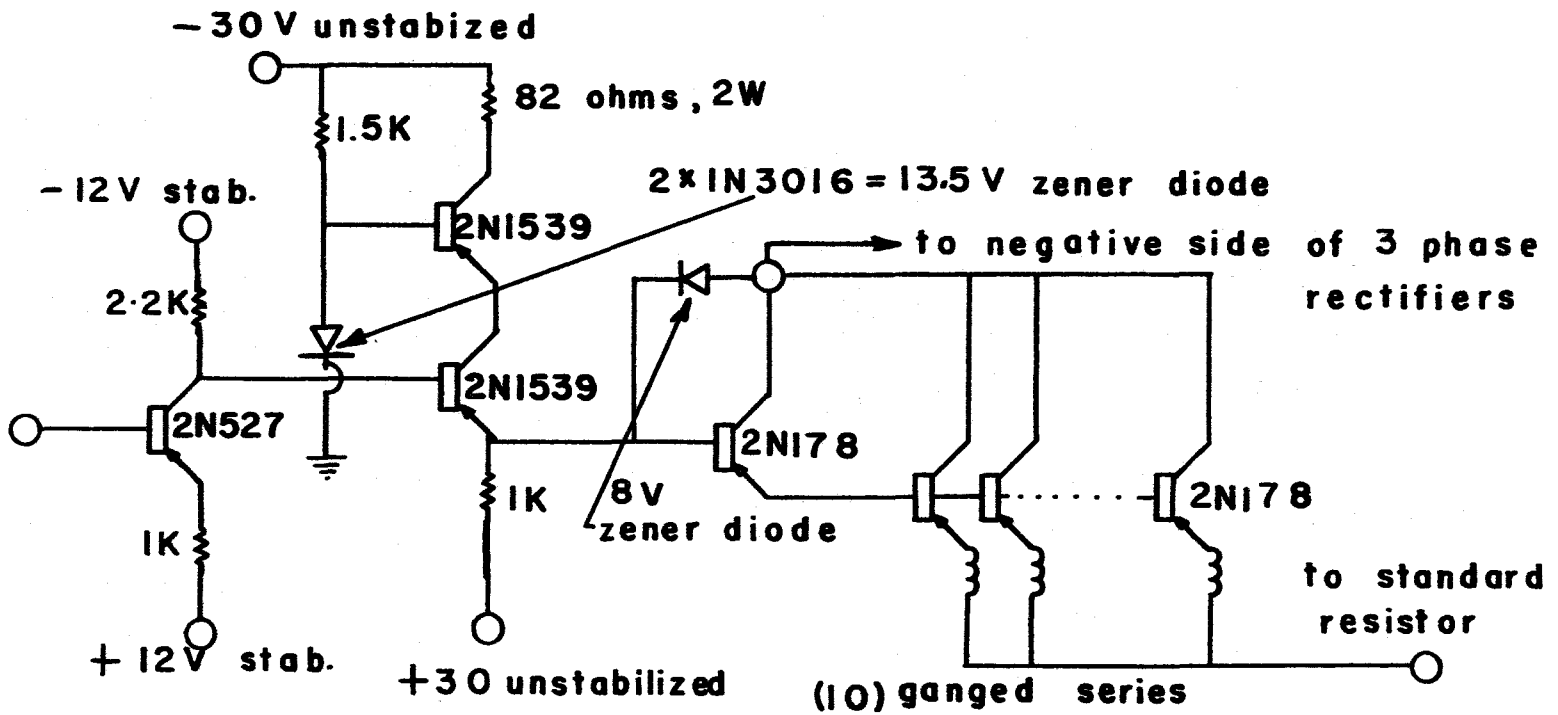

INVERTER POWER BOOSTER

FIGURE 3·3

or from 117 to 106. This is accomplished by using "ganged" zener diode construction as shown in Figure 3.2. Temperature stability is obtained by using temperature compensated zener diodes in the last two stages. Z_1 and Z_2 have temperature coefficients of 0.001%/C° and 0.005%/C° respectively.

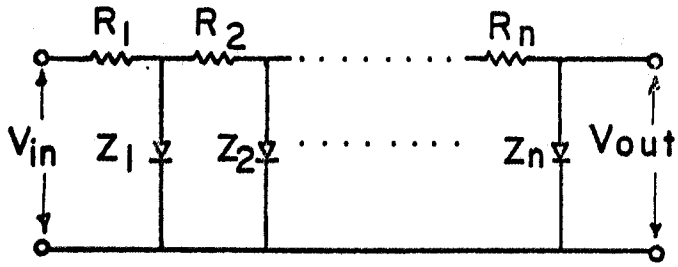

Figure 3.7 n Ganged Zener Diodes

The regulation for n ganged zener diodes (Figure 3.7) is easily calculated from the expression

$$\Delta V_{out} = \Delta V_{in}\left(\frac{r_1}{R_1}\right)\left(\frac{r_2}{R_2}\right)\cdots\left(\frac{r_n}{R_n}\right)$$

where ΔV_{out} is the output voltage change corresponding to an input voltage change of ΔV_{in}, $r_1, r_2, \cdots r_n$ are the dynamic impedences of the zener diodes $Z_1, Z_2, \cdots Z_n$ respectively. $R_1, R_2 \cdots R_n$ are the dropping resistors shown in Figure 3.7.

Using this expression two and three stage reference supplies were compared. It was found that sufficient regulation could only be achieved with a three stage supply. Temperature compensation was required in the second stage since the regulation factor (r_3/R_3) for the output stage was not sufficient to compensate for the thermal drifts of an "uncompensated" second stage zener diode.

(iii) The Fast Feedback System

As shown in Figure 3.1 the output from the reference supply is connected across a 10 turn, 100k logarithmic potentiometer. A Burr-Brown 1602/04 chopper stabilized operational amplifier compares the voltage across the standard resistor (Vba) with the voltage picked off from the logarithmic potentiometer (Vbc). The amplified difference signal (Vba-Vbc) is inverted and fed to a power booster stage (Figure 3.3). The output of the power stage is connected to the 10 parallel connected 2N278 series regulating transistors (Figure 3.3). The phase of the feedback signal is such as to reduce the difference (Vba-Vbc) to zero.

The system will exhibit high frequency oscillations unless ac. feedback is used to drop the gain of the operational amplifier at high frequencies. A Nyquist diagram could have been plotted to determine the feedback elements required for stability, but since a maximum ripple reduction and a low time constant were also required it was easier to set up the circuit and determine the feedback elements experimentally.

The standard resistor is made from constantan strip, wound non-inductively and is cooled by a 10 inch fan. The fan also provides cooling for the variacs, the rectifiers and the various power transistors.

(iv) The Servo System

The servo feedback system compares the voltage Vah, which is kept at 3 volts (Figure 3.4) and the voltage Vag, across the power transistors. The difference is chopped by the 60 cycle chopper and amplified (Figure 3.4) and then fed to the servo motor which controls the angular position of the three ganged variacs.

The amplifier consists of a difference amplifier T_1, T_2, and

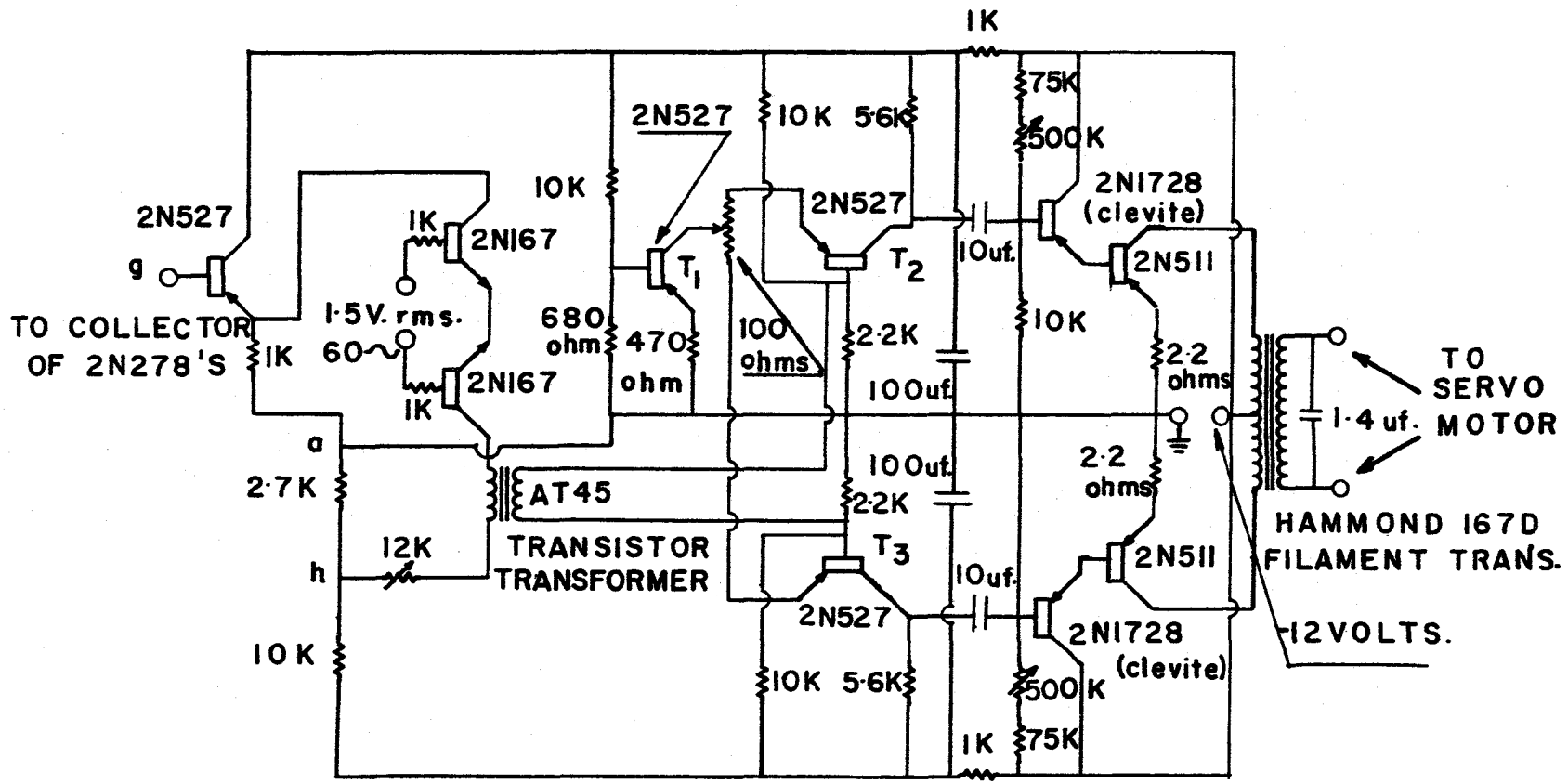

FIGURE 3·4 THE SERVO SYSTEM

T_3 (Figure 3.4) and a push-pull amplifier operating in class A-B mode. Biasing is controlled by the voltage on the base of the Clevite 1728 medium power transistors which drive the 2N511 output transistors. A tuned output transformer is used to convert the 60 cycle square wave to a 60 cycle sine wave for maximum response of the servo motor. The phase of the output signal from the chopper depends on the polarity of the dc. input signal to the chopper. The servo motor turns left or right depending on the phase and therefore upon the voltage across the power transistors. In this way 3 volts is kept across the 2N278's at all output currents.

(v) The Drive Mechanism

In chapter 1 section (iv) the response of a spectrometer to a monoergic beam was considered. If a plot is made of N(P)/P versus P the area under the curve was $\int \frac{N(P)}{P} dp = \omega \eta N(\xi_0)$ where N (ξ_0) is the peak counting rate and ω and η are constants. This indicates that all monoergic lines have the same shape in this type of plot. Since $\int \frac{N(P)}{P} dp = \int N(P)\, d(\log P)$ the same statement also applies to monoergic lines when N(P) versus log P is plotted.

The scanning mechanism contains the 10 turn 100k logarithmic potentiometer and a 15 turn 100k linear potentiometer connected by gears to the automatic scanning motor. A counter measures the rotational position of the logarithmic potentiometer. The schematic diagram of the scanning mechanism is shown in Figure 3.5.

The voltage Vbc picked off from the logarithmic potentiometer

is given by

$$V_{dc} = A e^{bx}$$

where A and b are constants and x is the rotational position of the logarithmic potentiometer measured from the bottom. The dial counter therefore measures x and we plot N(P) versus dial reading. To compare two different momenta only x and b are needed. The gearing between the logarithmic and linear potentiometer is such that the voltage picked off from the linear potentiometer is proportional to x. The output voltage from the linear potentiometer is used in conjunction with a x-y plotter for automatic plotting of the spectra. The x amplifier of the plotter is driven by the output of the linear potentiometer. Included in the scanning unit, but not connected by gears to the other potentiometers, is a linear 10 turn 100k helipot. It is connected as shown in Figure 3.5 and is used to shift the zero of the linear potentiometer. This feature allows expanded x scales on the x-y plotter to be used.

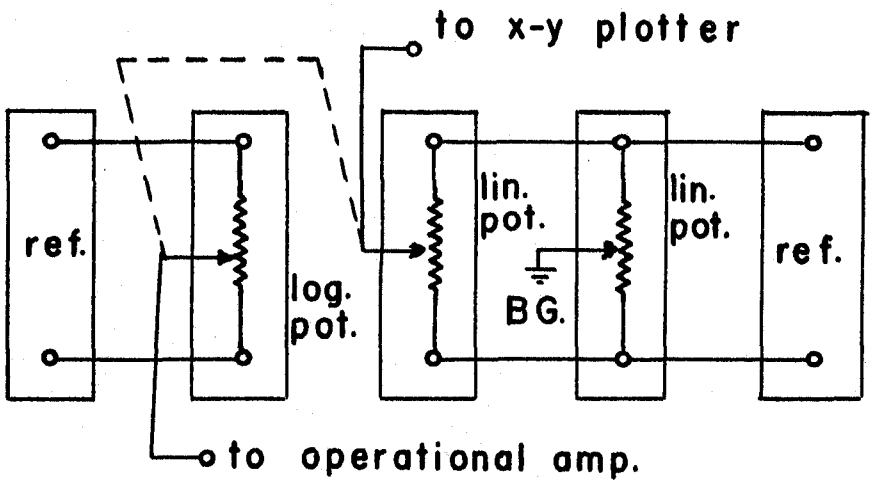

Figure 3.5 Schematic of Scanning Mechanism

(vi) The Local Power Supplies

There are three internal regulated power supplies. Each supply has an output ripple of less than 5 mv. at an output voltage of 12 volts. The circuit diagrams are given in Figure 3.6. The plus and minus

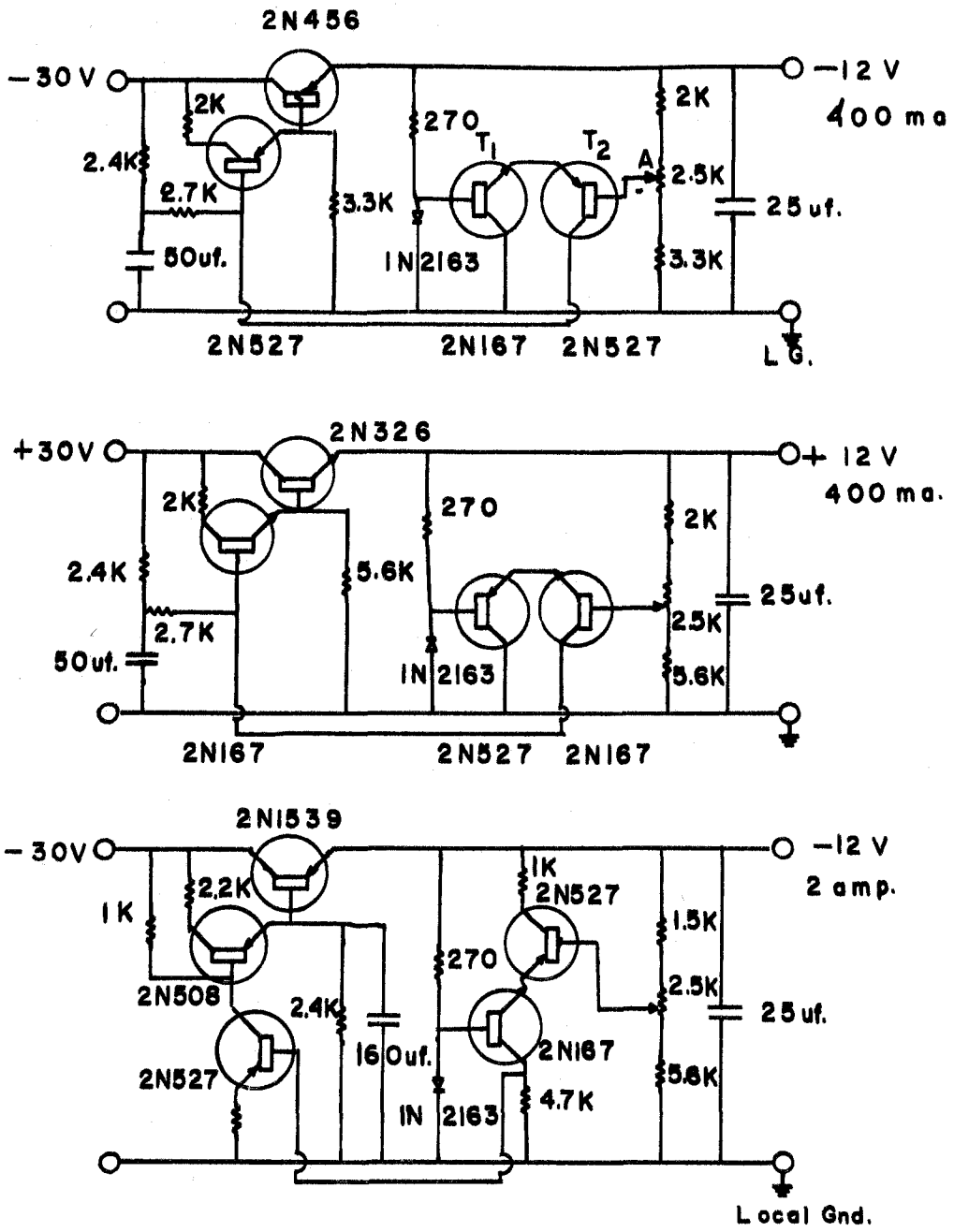

LOCAL POWER SUPPLIES

FIGURE 3·6

30 volts for the power booster are derived from the input filter to the three regulated supplies. The two plus and minus 12 volt 400 ma supplies are required for the operational amplifier and phase inverter while the minus 12 volt, 2 amp. supply is required for the servo system.

The operation of the supplies is similar to the operation of the current supply. Consider the minus 12 volt, 400 ma supply. The 2N456 is a series regulating transistor. The output voltage is sampled through a divider chain at point A and compared to a 1N2163 7 volt, temperature compensated zener diode reference, the difference is amplified by the cascaded difference amplifier (T_1 and T_2 Figure 3.6) and fed to the base of the 2N527 drives the 2N456. The operation of the plus 12 volt, 400 ma is the same. The minus 12 volt, 2 amp. supply has a 2N527 amplifying stage between the cascaded difference amplifier and the 2N508 driver.

(vii) Construction of the Current Supply

Plug in construction has been used to facilitate testing and servicing. There are five basic plug in units. These are (i) the drive mechanism, (2) the local power supplies, (3) the chopper and servo amplifier, (4) the Burr-Brown 1602/04 chopper stabilized operational amplifier, (5) the phase inverter and power booster. These units plug into a wiring panel. The drive mechanism may be mounted external to the supply. Lucite cards containing the ac. feedback components, the reference supplies, and the rectifiers for the local supplies are mounted on the wiring panel along with the various transformers and filter capacitors. The whole unit is housed in a 21" x 16" x 40" Hammond cabinet. A fan mounted on the top of the chassis forces air through it to provide cooling for the various components.

(viii) Tests on the Current Supply

(a) Regulation and Drift Tests

The voltage across the standard resistor was measured with a Leeds and Northrop potentiometer. The supply for the potentiometer was obtained from a 9.3 volt temperature compensated zener diode driven by a Hewlett Packard transistor power supply.

After the current supply had warmed up it was switched off for 30 minutes. When it was switched back on, the needle on the galvanometer returned to the same position it had been when the supply was switched off. This was repeated several times. This test indicates that there is negligible thermal drift in the supply and that it is exactly repeatable.

Using another set of ganged General Radio variacs the input voltage to the supply was varied from 106 to 128 volts. The resulting deflection of the galvanometer needle indicated a change in output current of less than 0.01%.

(b) Test on the Line Widths and Linearity of the Supply

A thin Th(B - C - C") source was prepared by collecting the charged ions on a thin mylar foil at 150 volts. The mylar was masked so that a 2mm source was obtained. The source holder for β- γ angular was used. The source was centered using the F line. With the photomultiplier running at 2,000 volts the accelerating and deflection and accelerating electrode potentials were adjusted as described in chapter IV section (vi). The output from the photomultiplier was amplified and then fed to a pulse height analyser to discriminate against noise. The pulses from the pulse height analyser were then counted with Phillips counting equipment. The counting rates at several points on the F, I, L,

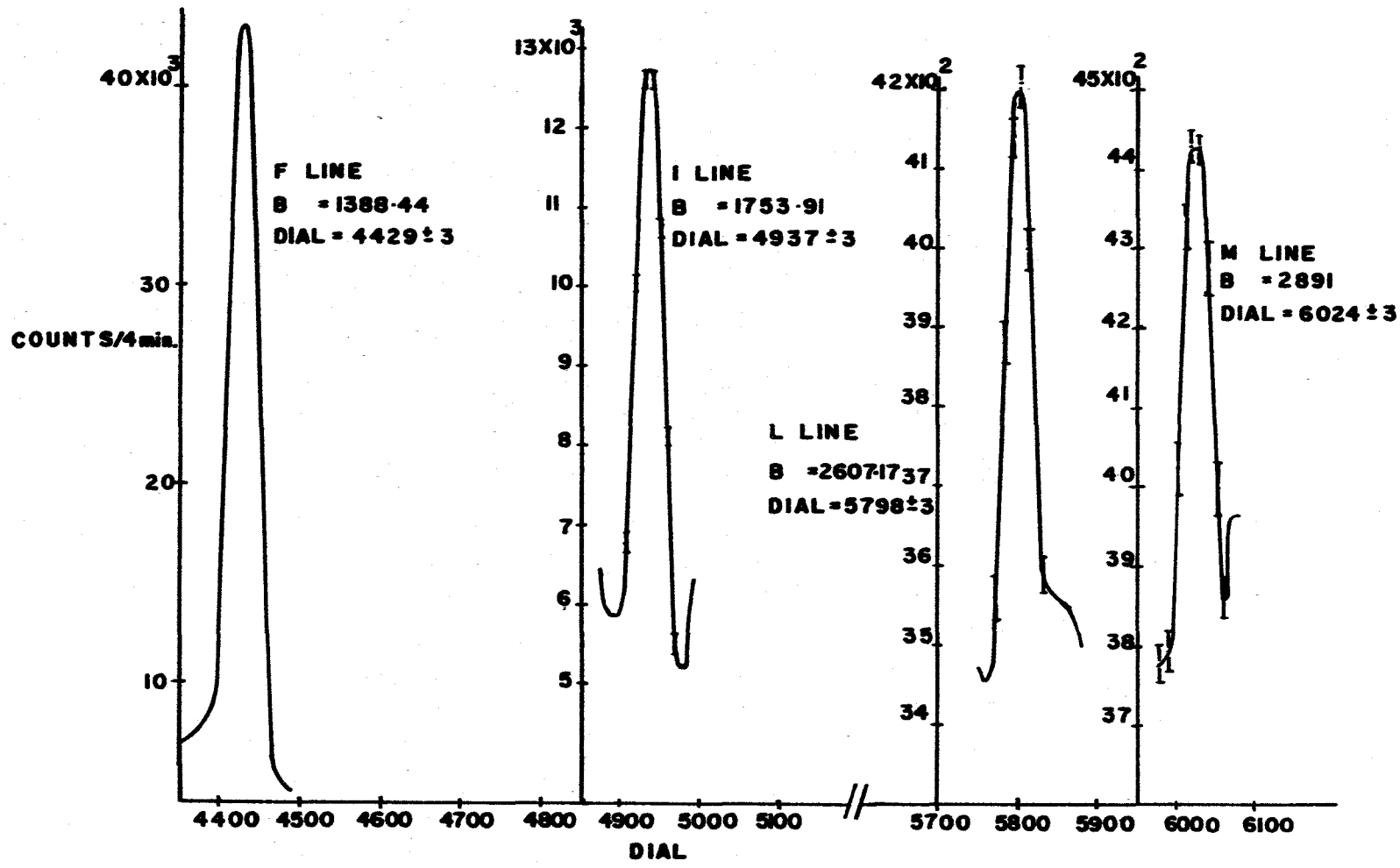

FIGURE 3·8 The F, I, L and M lines of Thorium

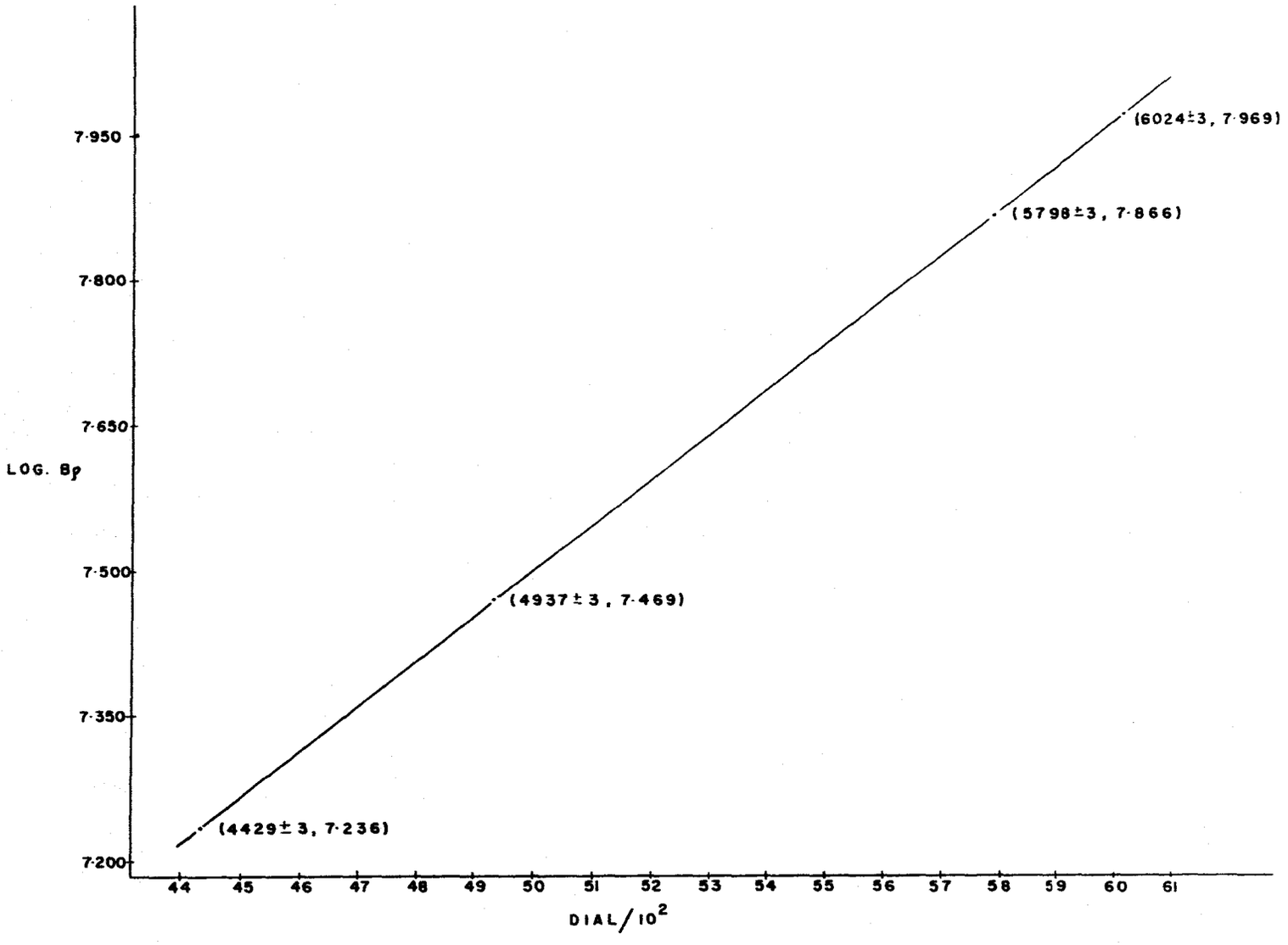

FIGURE 3·9 LOG Bp VERSUS DIAL

and M lines were taken manually. In addition these lines were scanned automatically by feeding the pulse height analyser output to a rate-meter and then to the y amplifier of an x-y plotter. The x amplifier was driven with the output from the linear potentiometer (Figure 3.5). The lines (Figure 3.8) were found to have the same shape and have a 2% resolution.

Figure 3.9 is the plot of the logarithm of $B\rho$ versus the dial setting for the four lines measured. The points fall on a straight line which indicates that the dial setting is proportional to the logarithm of the momentum focussed. The momentum focussed is therefore given by the relation

$$B\rho = A e^{bx}$$

where A and b are constants and x is the dial setting. Comparing two lines gives $b = 0.4605 \pm 0.0008) \times 10^{-3}$. b was also determined by plotting the logarithm of the spectrometer current versus dial setting. The value obtained was $b = (0.4606 \pm 0.0006) \times 10^{-3}$.

CHAPTER IV

THE COINCIDENCE METHOD

(i) Introduction

In Figure 4.1 is represented schematically a simple beta decay. The parent decays by beta emission to an excited state of the daughter. Assuming lifetimes of excited states are very short

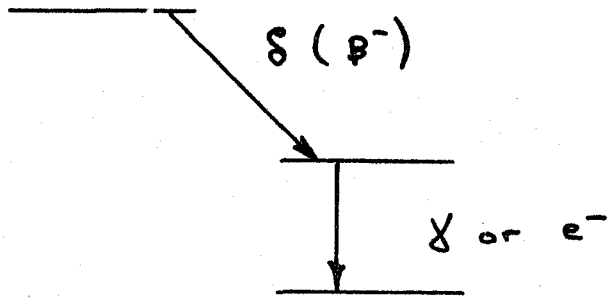

Figure 4.1 Simple Decay Scheme

coincidences can be recorded between these beta particles and the subsequently emitted gamma ray or conversion electrons. Electron beta (e-β) and electron-electron (e-e) coincidences can be studied with two magnetic lenses. With one magnetic lens replaced by a scintillation spectrometer, beta-gamma (β-γ) and electron-gamma (e-γ) coincidence experiments can be done.

(ii) e-β Coincidences

e-β coincidences are studied with one spectrometer focussed on the peak of the conversion line, while the other one scans the beta continuum. The spectrum of beta rays in coincidence with the conversion line is obtained. A Fermi plot will indicate if the spectrum is simple

or complex. Figure 4.1 represents the simple case while Figure 4.2 represents the complex case. If we study a complex case, the area under the total coincidence spectrum, when combined with the area under the total single channel spectrum, will yield the branching ratio δ or the conversion probability K (of the beta group or the conversion electron respectively) depending on which one of these is known.

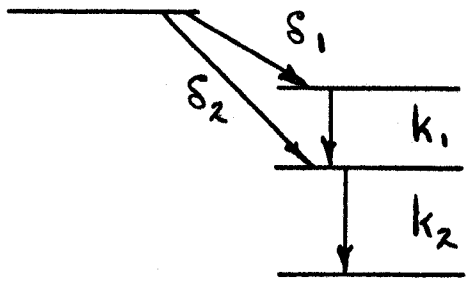

Figure 4.2 Complex Decay Scheme

Consider the complex case of Figure 4.2. We will consider the case of spectrometer number 1 focussed on the conversion line K_1 of momentum P_1 while spectrometer number 2 is focussed on the continuum at momentum P_2. The single channel counting rates will be

$$N_1 = N_0 \phi(P_1) \omega_1 \eta_1 P_1 + N_0 \delta_1 \omega_1 k_1$$

$$N_2 = N_0 \phi(P_2) \omega_2 \eta_2 P_2$$

where we have adopted the results and symbols of chapter 1. $N_0 \delta_1$ is the intensity of the B_1 group and K_1 is the conversion probability. The number of conversion electrons per beta disintegration is $\delta_1 k_1$. Denote by ϕ_1 the spectrum shape factor for the partial spectrum δ_1. The counting rate due to the δ_1 spectrum is then given by

$$N_0 \delta_1 \phi_1(P_2) \omega_2 \eta_2 P_2$$

Spectrometer number 1 sees only $\omega_1 k_1$ of these as conversion electrons. Therefore, the coincidence counting rate is

$$N_c = N_0 \delta_1 \phi_1(P_2) \omega_2 \eta_2 P_2 \omega_1 k_1$$

If we plot N_c/P_2 versus P_2 then the area under the curve is

$$A_c = \int \frac{N_0 S_1 \phi_1(P_2) \omega_2 \eta_2 P_2 \omega_1 k_1 \, dP_2}{P_2}$$

$$= N_0 S_1 \omega_1 \omega_2 \eta_2 k_1$$

Combining this with the area under a singles curve we get

$$\frac{A_c}{A_s} = \frac{N_0 S_1 \omega_1 \omega_2 \eta_2 k_1}{N_c \eta_2 \omega_2} = S_1 \omega_1 k_1$$

We can find S_1 or k_1 easily by measuring A_c/A_s, ω_1 and one of S_1 or k_1. If the excited levels decay by more than one process then the above results must be multiplied by a factor equal to the branching ratio for transition from this level.

(iii) e-e Coincidences

In e-e coincidence experiments, one spectrometer is focussed on one peak while the other spectrometer scans the other peak. The conversion lines are, however, in coincidence with partial beta spectra. The coincidence counting rate will be

$$N_c = N_c(k_1 k_2) + N_c(k_1 \beta) + N_c(k_2 \beta)$$

$N_c(k_1 \beta)$ and $N_c(k_2 \beta)$ are found by taking coincidence counts with one spectrometer "on" its line while the other is "off" the line.

The coincidence counting rate due to two transitions such as in Figure 4.2 is

$$N_c(k_1 k_2) = N_0 S_1 \omega_1 k_1 \omega_2 k_2$$

The single channel peak height due to the k_1 conversion line is

$$N(k_1) = N_0 S_1 k_1 \omega_1 .$$

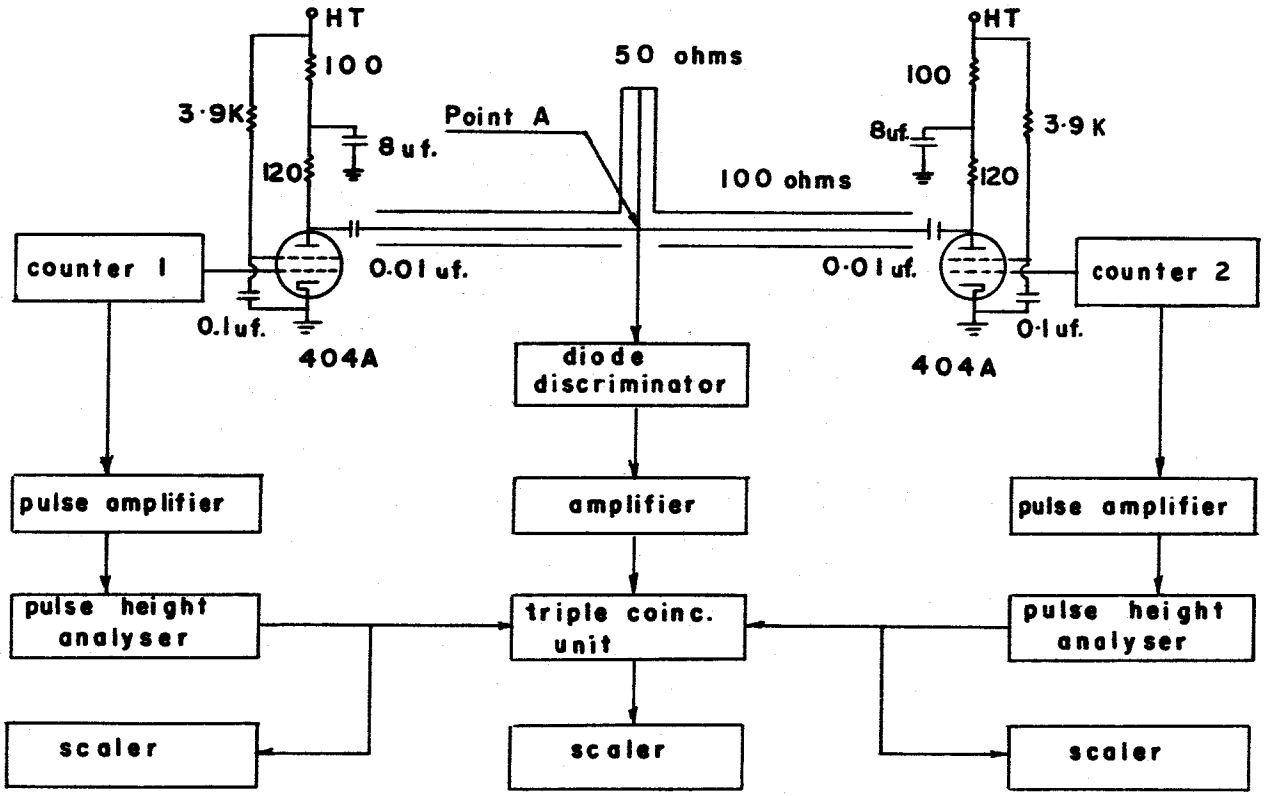

FIGURE 4·3 The Bell, Graham and Petch "Fast-Slow" Coincidence Circuit.

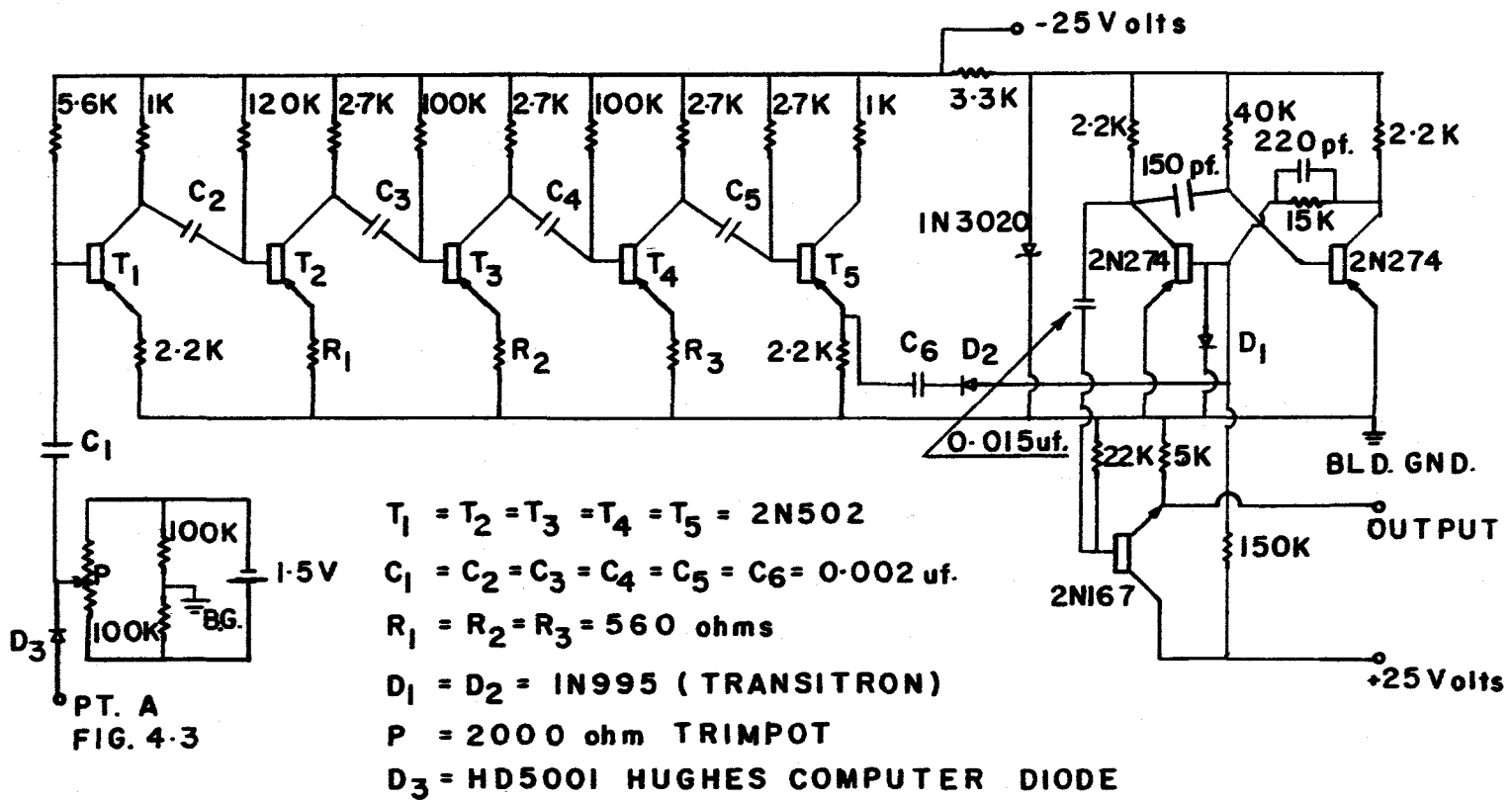

FIG. 4·3

$T_1 = T_2 = T_3 = T_4 = T_5$ = 2N502

$C_1 = C_2 = C_3 = C_4 = C_5 = C_6$ = 0·002 uf.

$R_1 = R_2 = R_3$ = 560 ohms

$D_1 = D_2$ = IN995 (TRANSITRON)

P = 2000 ohm TRIMPOT

D_3 = HD5001 HUGHES COMPUTER DIODE

FIGURE 4·4 THE FAST CIRCUIT

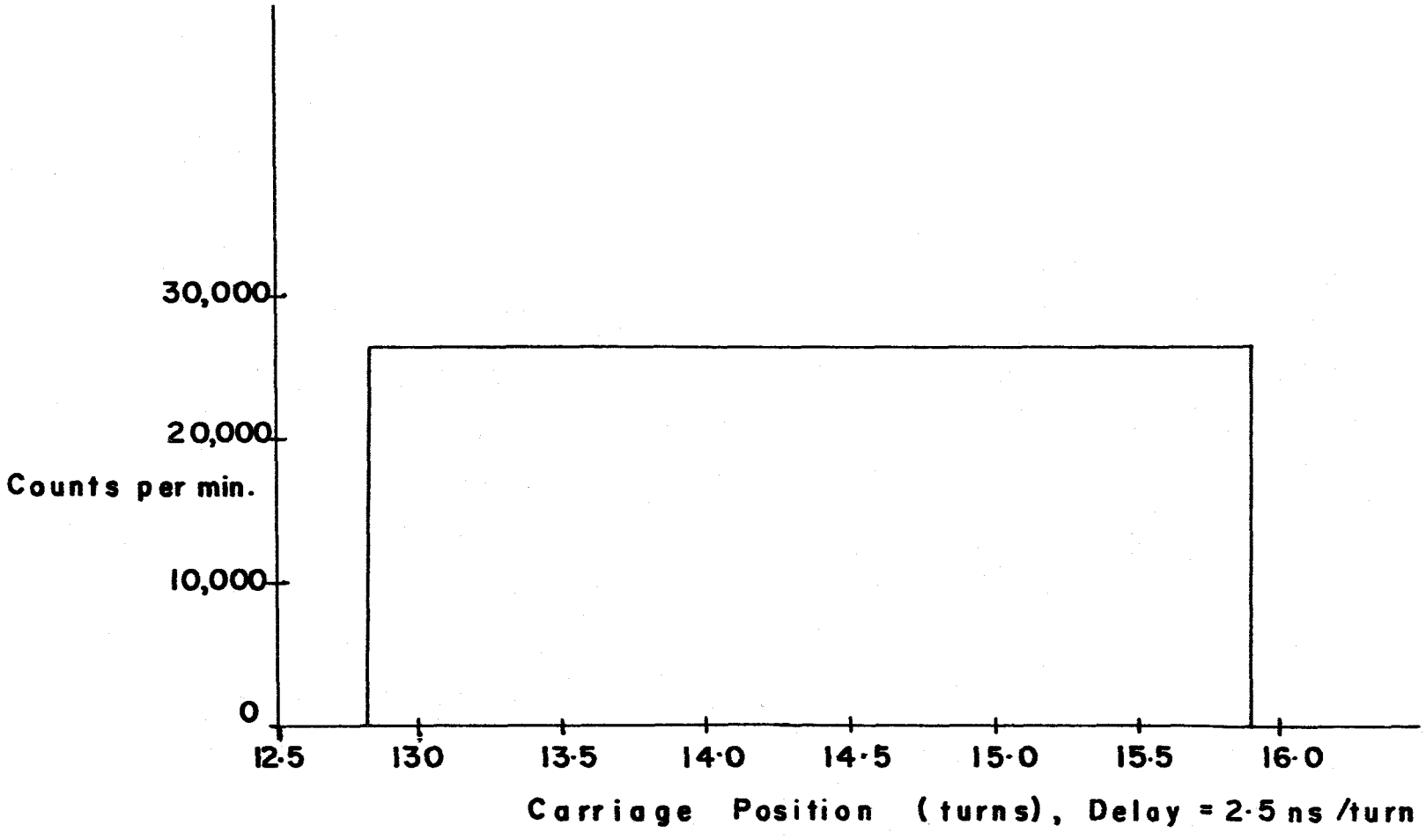

FIGURE 4·5 Prompt Coincidence Curve

Then

$$\frac{N(k_1, k_2)}{N(k_1)} = \omega_2 k_2$$

This gives the conversion probability k_2 since ω_2 is measurable. If we study e-B and e-e experiments from the same source, the ratios $\omega_1 k_1$ and $\delta_1 \omega_1 k_1$ will yield δ_1 directly.

(iv) β-γ Coincidences

The analysis of this case is essentially the same as in the e-β case. If we assume a detection efficiency ε and accept the photopeak only, then we simply replace $\omega_1 k_1$ by $\omega_\gamma k_\gamma \varepsilon$. ω_γ is now the solid angle accepted by the gamma spectrometer and k_γ is the probability for gamma emission. $\omega_\gamma k_\gamma \varepsilon$ is the number of gammas counted per each δ_1 disintegration.

(v) Description of our Fast Coincidence Circuit

Bell, Graham and Petch (1949, 1952) have described a "fast-slow" coincidence circuit which uses a helical- coiled coaxial line to provide a variable delay between two counters. A diagram of our circuit, which is formally the same as theirs, is given in Figure 4.3. Negative pulses from the photomultiplier tube cut off a 404A pentode, thus producing a positive 3 volt pulse across a 100 ohm resistor. Since the photomultipliers are run at 2,000 volts, the leading edge of this pulse is due to the first photoelectron released from the photocathode. These fast pulses are then fed through 100 ohm coaxial cable to one end of the helical delay line. The clipping cable has an impedence of 50 ohms so that pulses reflected from its short circuited end are terminated properly at point A. From point A the clipped pulses are fed to a solid state diode discriminator. The diode is biased to accept only double

pulses (coincidences) appearing at point A. The pulse from the diode goes to a three stage transistor pulse amplifier and then to a saturated monostable multivibrator. The multivibrator gives out a 6 volt 3 microsecond pulse, which goes to the "slow" triple coincidence circuit. Figure 4.4 shows the electronics described above. Saturation in the multivibrator is important in order to eliminate spurious pulses originating from noise and pickup.

We have obtained resolving times of the order of 10^{-9} seconds using a Tektronics pulse generator. The prompt coincidence curve of Figure 4.5 were obtained using a 4 nanosecond clipping cable and pulses from the Tektronics pulse generator. The time delay between the "on" and "off" states is of the order of 5×10^{-12} seconds.

(vi) Adjustment of the "Fast-Slow" Coincidence Circuit

With the source centered the beta spectrometer was focussed on the energy to be used in the experiment. The focussing electrode on the gamma and beta detectors were adjusted by observing that no further increase in pulse height was obtained. In this way only a small section of the photocathode was used. The deflection electrode on each detector was adjusted to obtain a maximum output voltage. The beta single channel pulse height analyser was set to discriminate against noise and the gamma single channel pulse height analyser was set to take in the 511 kev. and 600 kev. photopeaks.

The diode bias and carriage position were set to approximate values. A diode bias curve (Figure 4.6) was taken. This is obtained by plotting the doubles count rate versus diode voltage. The diode operating point was chosen in the centre of the flat portion of the curve.

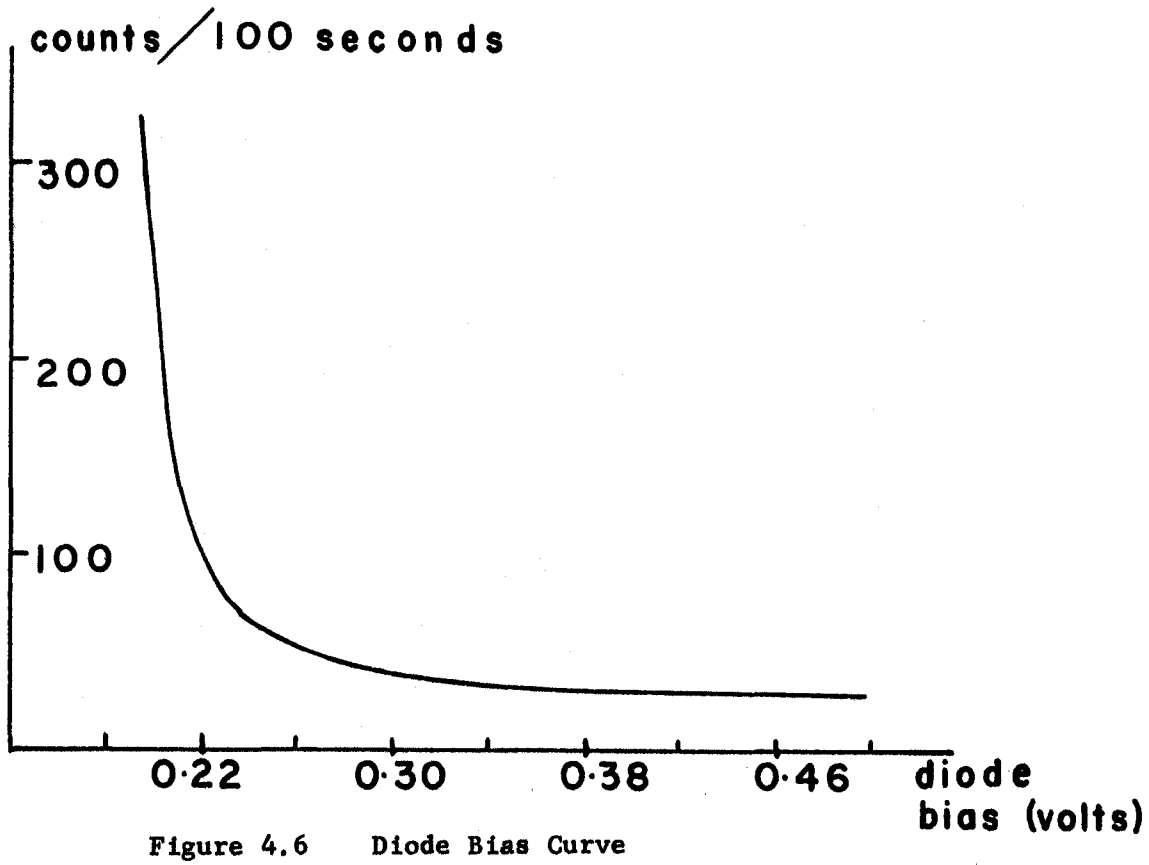

Figure 4.6 Diode Bias Curve

A prompt coincidence curve was next taken. This was obtained by taking the doubles count rate at various delays of one channel with respect to the other. The carriage was set to a position corresponding to the middle of the prompt coincidence curve.

CHAPTER V

THE As^{74} EXPERIMENT

(i) Introduction

The decay scheme of As^{74} is shown in Figure 5.1. We have studied the beta gamma angular correlation between the 0.93 mev. positron group and the subsequent 600 kev. gamma ray at the beta energies of w = 1.8, 2.0, 2.2, 2.4 and 2.6 (relativistic units). The decay is similar to the decay of As^{76} studied by Matumoto, Yamada, Wang and Morita (1963). If the modified Bij approximation applies to the As^{74} case then the structure of the low lying 2^+ state of Ge^{74} can be found.

(ii) Procedure

The apparatus was checked by measuring the beta-gamma angular correlation of Co^{60} which is known to be isotropic. We obtained an A_2 coefficient of $(0.75 \pm 6.3) \times 10^{-3}$. This indicates that the equipment will not introduce an anisotropy into an experiment provided the gain of the gamma spectrometer does not change when rotated between the 90^o and the 180^o position.

A thin source was prepared by evaporating a solution containing the As^{74} on a thin, aluminum coated, mylar foil that had been wetted by insulin. The size of the source was determined by the area wetted. The source position was adjusted so that a maximum counting rate was obtained in the beta channel. The gamma spectrometer was adjusted so that the axis of rotation passed through the source position. The"fast slow" coincidence circuit was adjusted as described in chapter IV.

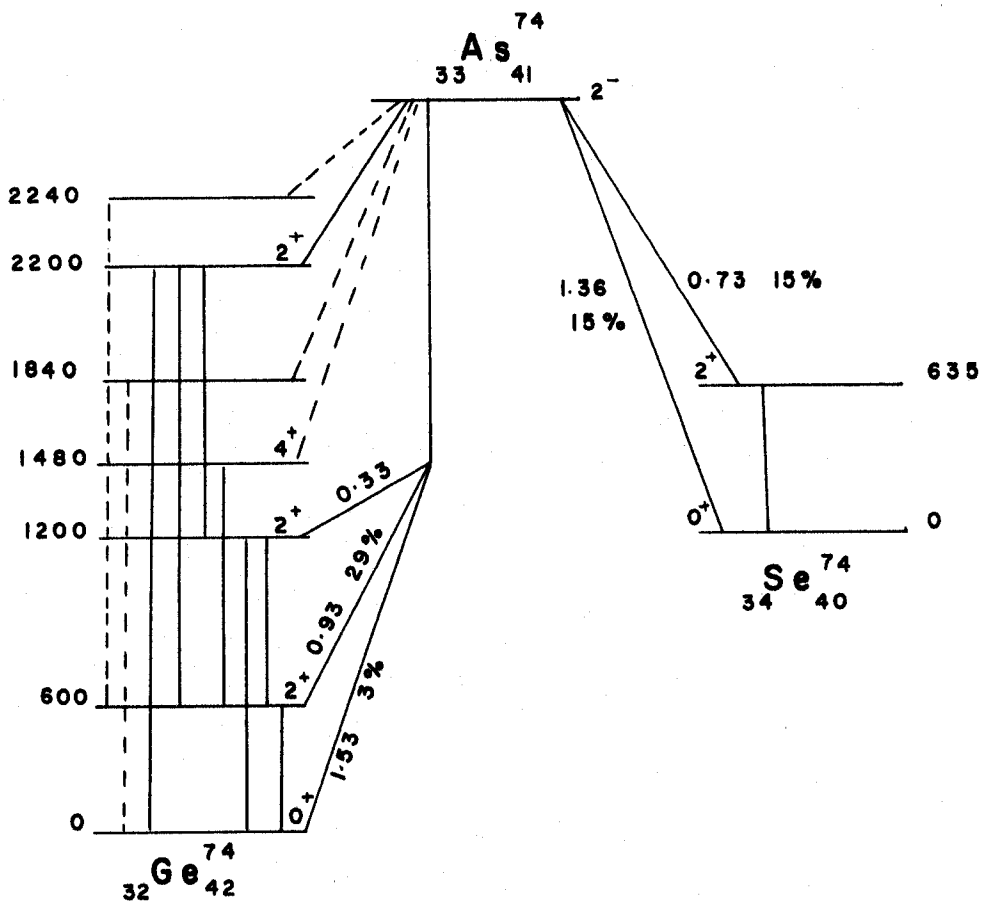

FIGURE 5·1 The As^{74} Decay Scheme

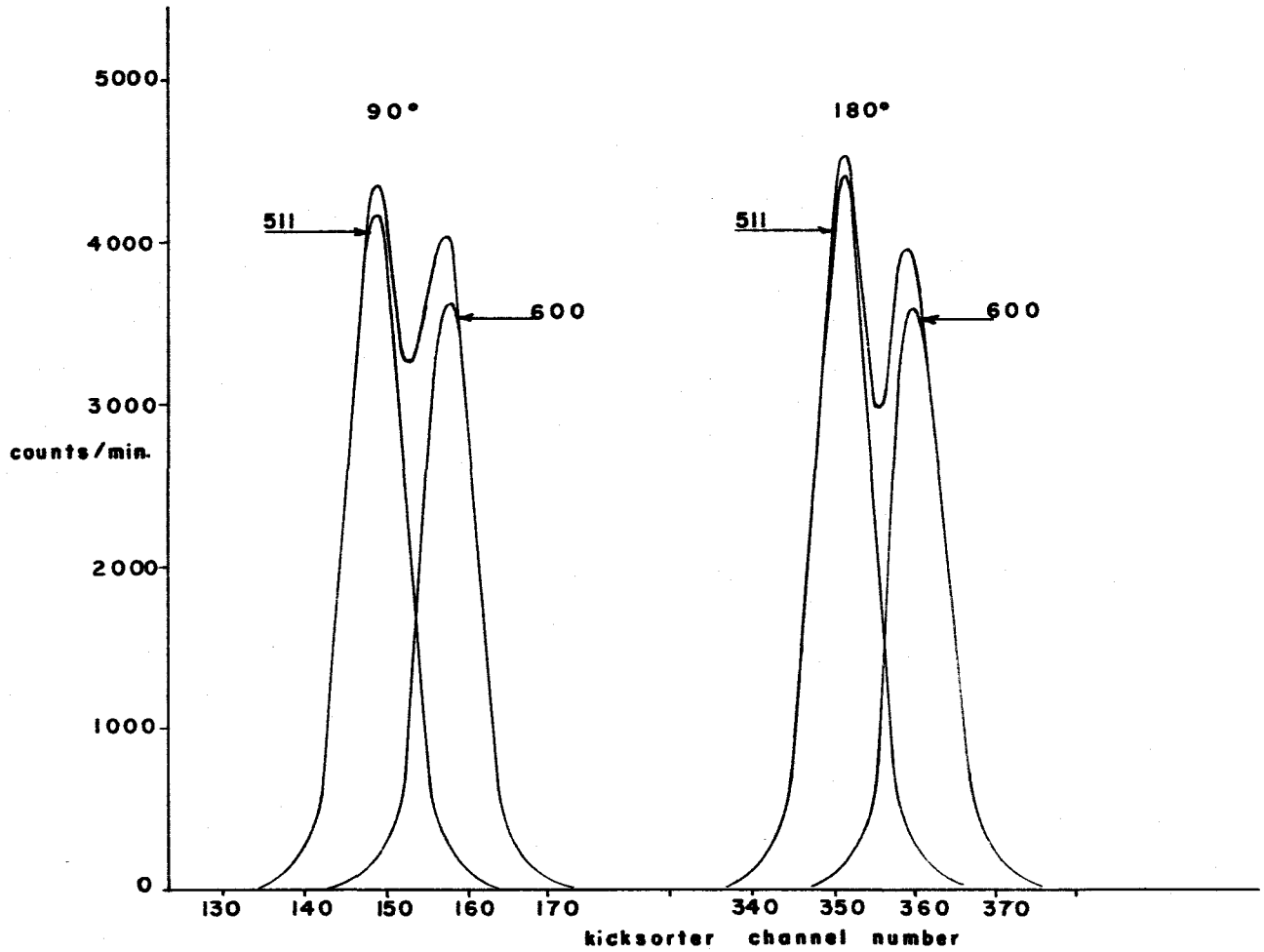

FIGURE 5·2 THE 511 kev. and 600 kev. PHOTOPEAKS

The gamma single channel pulse height analyser was set to take in the 600 kev. photopeak and a large portion of the compton continuum. The 511 kev. annihilation gamma was therefore taken in also. Figure 5.2 is a plot of the gamma spectrum. The spectrum was monitored with the kicksorter every three hours. The single channel pulse height analyser is the beta channel was set to discriminate against noise. The triple coincidences, the beta singles and the gamma singles were counted for twenty minute intervals automatically by Phillips counting equipment. The scintillation spectrometer was moved very three hours between the 90 and 180 degree positions.

(iii) Interpretation of Results

The triple coincidence counts were normalized with respect to the corresponding gamma channel singles count. The logarithm of the gamma singles were also plotted versus time. All counts which deviated by more than 1% from the mean were excluded. With the baffles in the beta spectrometer closed the contributed to the triple coincidence count rate, due to scattering, was measured. Values obtained were as follows: 2.18 ± 0.46 counts per 10^6 gamma singles at 90°; 3.71 ± 0.56 counts per 10^6 gamma singles at 180°.

In Figure 5.2 it can be seen that the ratio of the 511 kev. peak to the 600 kev. peak varies with scintillation spectrometer position.

The coincidence counting rates at 90° and 180° are given by

$$N(90) = XA + YB$$

$$N(180) = X_1A_1 + Y_1B_1$$

where A and A_1 are the total counts due to the 600 kev. transition at 90° and 180° respectively, B and B_1 are the total counts due to the 511 kev. annihilation gammas at 90° and 180° respectively. X, X_1, Y and Y_1

are constants.

XA and X_1A_1 are the true triple coincidence counts while YB and Y_1B_1 are triple coincidence counts due to scattering of the 511 kev. annihilation gammas. Each triple coincidence count was normalized with respect to the corresponding gamma singles count. Thus we obtained, normalizing to a gamma singles count T,

$$\frac{N\ (90)\ (T)}{A + B} = \frac{X\ A\ T}{A + B} + \frac{Y\ B\ T}{A + B}$$

$$\frac{N\ (180)\ (T)}{A_1 + B_1} = \frac{X_1\ A_1\ T}{A + B} + \frac{Y_1\ B_1\ T}{A_1 + B_1}$$

We want to obtain X_1T and XT. From the expression above we have

$$XT = \frac{A + B}{A}\left[\frac{N\ (90)\ (T)}{A + B} - \frac{Y\ B\ T}{A + B}\right]$$

$$X_1T = \frac{A_1 + B_1}{A_1}\left[\frac{N\ (180)\ (T)}{A_1 + B_1} - \frac{Y_1\ B_1\ T}{A_1 + B_1}\right]$$

$\frac{Y\ B\ T}{A + B}$ and $\frac{Y_1\ B_1\ T}{A_1 + B_1}$ were measured

and subtracted from the normalized triple coincidence counting rates. To find $(A + B)/A$ and $(A_1 + B_1)/A_1$ we need to know the ratio $B / A = m$ and $B_1 / A_1 = n$. Then $(A + B)/A = 1 + m$ and $(A_1 + B_1)/A_1 = 1 + n$. m and n were found by measuring the areas under the 511 kev. and 600 kev. peaks shown in Figure 5.2. The values obtained were $m = 1.20 \pm 0.07$ $n = 1.12 \pm 0.07$. Table II gives the corrected results.

TABLE II

W	A_2	$\pm$
1.8	0.0437	0.0055
2.0	0.0045	0.00051
2.2	-0.0365	0.0072
2.4	-0.024	0.0092
2.6	-0.168	0.123

The w = 1.8 run is unreliable since a great many of the counts had to be discarded. This was attributed to the Phillips counting equipment which was not working properly. The counting rate for the w = 2.6 run was low. A large correction, due to scattering, had to be made. For example, the total number of counts were 6068 at 180° while a correction applied to this figure was 2345 counts.

The scattering corrections are also suspected to be unreliable. They were measured with the spectrometer focussing negatrons. In this mode the positrons collide with the positron baffle at a position near the source end of the spectrometer. However, with the spectrometer current reversed the positrons collide with the Hubert baffle. Thus, the source of the annihilation gammas is considerably changed in the positron experiment. The scattering results for the negatron experiment may not be applicable to this experiment, especially when large corrections have to be made as in the w = 2.6 case.

CONCLUSION

To improve the coincidence count rate a large portion of the Compton continuum of the 511 kev. and 600 kev. photopeaks was taken in. To find m and n, however, only the areas under the photopeaks were compared. The 600 kev. peak was considered as one peak although it consists of two closely spaced peaks of 600 kev. and 635 kev. Thus, there are uncertainties in the determination of m and n. Because of these uncertainties the errors quoted in the results are suspect.

The experiment could be repeated to eliminate these uncertainties. The photomultiplier of the scintillation spectrometer has been shielded so that changes in peak position, as seen in Figure 5.2, are negligible.when the spectrometer is shifted between the 90^{o} and 180^{o} positions. The voltage and centre of rotation of the scintillation spectrometer should be adjusted such that the trailing edge of the 600 kev. photopeak as measured at the 90^{o} position coincides with its trailing edge as measured at the 180^{o} position. The whole gamma spectrum should be taken in to improve the triple coincidence count rate which can be normalized with respect to time, since the decay constant is known. Corrections for scattering of the 511 kev. annihilation gammas should be measured while the beta spectrometer is focussing positrons.

Alternatively, the resolution of the scintillation spectrometer could be decreased from its value of 16% to 10%. The 511 kev. and 600 kev. peaks would be cleanly resolved and the gamma single channel pulse height analyser could be set to bracket the 600 kev. peak.

Although the coincidence count rate would be reduced, the need for correcting, due to scattering of the 511 kev. annihilation gammas would be eliminated. Centering of the spectrometer would be simplified and normalization of the coincidence rates could be done with respect to the gamma singles.

Discarding the results at W = 1.8 and 2.6, the W = 2.0, 2.2 and 2.4 results indicate that the anisotropy is small. There is, therefore, no strong K forbiddeness or j selection rule to limit the contribution from matrix elements other than $\int$Bij.

BIBLIOGRAPHY

Alaga, Alder, Bohr and Mottelson 1955. Kgl. Danske Videnskab. Videnskab. Selskab, Mati-fys. Medd. 29, No. 9.

Bell, R.E., Graham, R.L. and Petch, H.E. 1952. Can. Jour. Phys. 30, 35.

Bell, R.E. and Petch, H.E. 1949. Phys. Rev. 76, 1409.

Busch, H. 1926. Ann. Physik 81, 974; 1927. Arch. Electrot. 18, 583.

Falkoff, D.L. and Uhlenbeck, G.E. 1950. Phys. Rev. 79, 334.

Gerholm, T.R. 1956. Ark. f. Fysik 11, No. 2, 55.

Hartwig, G. and Schopper, H. 1960. Rev. Letters 4, 293.

Hubert, P. 1952. Physica XVIII, No. 12.

Konopinski, E.J. 1959. Ann. Rev. Nuclear Sci. 9, 99.

Kotani, T. 1959. Phys. Rev. 114, 795.

Lindgren, J. 1958. Nuclear Instruments 3, 104.

Matumoto, Z., Morita, M. and Yamada, M. 1955. Bull. Kobayasi Inst. Phys. Research 5, 210.

Matumoto, Z., Yamada, M., Wang, I-T. and Morita, M. 1963. Phys. Rev. 129, 1308.

Morita, M. and Morita, R.S. 1958. Phys. Rev. 109, 2048.

Siegbahn, K. 1955. Beta and Gamma Ray Spectroscopy, chapter III.

Siegbahn, K. 1946. Phil. Mag. 37, 162.

Slatis, H. and Siegbahn, K. 1949. Ark. f. Fysik I, Nr. 17, 339.

Steffen, R.M. 1960. Phys. Rev. Letters 4, 290; 118, 763.

Weidenmuller, H.A. 1961. Revs. Modern Phys. 33, 574.

VITA AUCTORIS

1938, February 8	Born at Windsor, Ontario
1957	Senior Matriculation from Walkerville Collegiate, Windsor, Ontario.
1962	Bachelor of Science Degree from Assumption University of Windsor.
	Awarded National Research Council Scholarship for study at Assumption University of Windsor.
1963	Master of Science Degree expected from Assumption University of Windsor.
	Awarded National Research Council Scholarship for study at McGill University.